A criterion characterizing accumulated neurotoxicity of Aβ oligomers in Alzheimer's disease

Andrey V. Kuznetsov

Department of Mechanical and Aerospace Engineering, North Carolina State University,

Raleigh, NC 27695-7910, USA; e-mail: avkuznet@ncsu.edu

Abstract

The paper develops a criterion to quantify the accumulated neurotoxicity of Aβ oligomers in Alzheimer's disease (AD). Accumulated neurotoxicity is determined by integrating the concentration of Aβ oligomers within the control volume over time. In the scenario of a low rate of free Aβ oligomer deposition into senile plaques and dysfunctional degradation machinery, resulting in an infinitely long half-life of Aβ monomers and aggregates, the obtained analytical solution reveals a quadratic relationship between accumulated neurotoxicity and time. This suggests that initially, the neurotoxicity increases slowly but accelerates as time progresses. This could help to understand the prolonged delay in the onset of AD symptoms. Furthermore, as the model indicates that accumulated neurotoxicity increases with the duration of the aggregation process, it implies that if the protein degradation system is compromised, the onset of AD becomes unavoidable. Eventually, neuronal death is only a question of time. The only way to prevent this outcome is to ensure that the degradation machinery for Aβ peptides and their aggregates remains functional. A threshold value of accumulated neurotoxicity is suggested. If this value is exceeded, nearby neurons die. The progression of accumulated neurotoxicity over time is analyzed. An S-shaped growth pattern as the half-deposition time of Aβ aggregates into senile plaques increases is revealed. Additionally, the sensitivity of accumulated neurotoxicity to different parameter values is examined.

Keywords: neuron; Alzheimer's disease; Finke−Watzky model, mathematical modeling; polymerization

Abbreviations

Aβ	amyloid beta
AD	Alzheimer's disease
CV	control volume
F-W	Finke-Watzky

1. Introduction

Alzheimer's disease (AD) is a progressive neurodegenerative disorder and the leading cause of dementia, characterized by extracellular amyloid beta (Aβ) plaques and intracellular tau tangles. The disease significantly impacts daily life and independence [1-5].

AD involves the aggregation of Aβ peptides into fibrillar structures through secondary nucleation, an autocatalytic process [6]. Aβ monomers are generated by the cleavage of amyloid precursor protein (APP) by β- and γ-secretases, a process that occurs on lipid membranes [7,8]. Most Aβ monomers are then released into the extracellular space, where they can aggregate [9].

The "neurotoxic (hereafter toxic) Aβ oligomer" hypothesis suggests that small, soluble oligomers of amyloid peptides cause cellular toxicity, providing a potential explanation for the weak correlation between amyloid plaques and neurodegeneration in AD. In this hypothesis, Aβ plaques are considered relatively inert sinks of toxic intermediate species [10]. Aβ monomers also exhibit minimal toxic activity [11]. The primary hypothesis for AD toxicity is that toxic Aβ oligomers disrupt the neuronal membrane [12]. However, the absence of a quantifiable parameter characterizing oligomer toxicity complicates the determination of a toxic threshold that must be exceeded for neuronal death processes to begin [10].

Mathematical models exploring the mechanisms behind Aβ plaque formation were developed in [13-16]. The Finke-Watzky (F-W) two-step model [17] was employed to simulate Aβ aggregation. Building on this foundation, the present paper introduces a model for calculating the accumulated toxicity of Aβ oligomers. Both numerical and analytical solutions are presented to clarify how accumulated toxicity depends on disease duration and various biophysical processes represented by the model parameters.

2. Materials and models

2.1. Equations of the mathematical model

The F-W model represents a simplified two-step mechanism for aggregate formation, comprising nucleation and autocatalysis. In the nucleation step, new aggregates form continuously, while in the autocatalysis step, existing aggregates facilitate their own further production [17,18]. The model outlines these two pseudo-elementary reaction steps as follows:

$$A \xrightarrow{k_1} B \tag{1}$$

$$A + B \xrightarrow{k_2} 2B \tag{2}$$

Here, A represents a monomeric peptide, while B represents a free (not yet deposited into a plaque) amyloid-converted peptide. The kinetic constants k_1 and k_2 denote the rates of nucleation and autocatalytic growth, respectively [17]. Primary nucleation, described by Eq. (1), involves only monomers, whereas secondary nucleation, described by Eq. (2), includes both monomers and existing free aggregates of the same peptide [6].

If Aβ monomers diffuse rapidly, the concentration of Aβ monomers, C_A, is nearly uniform in the CV. In this scenario, time, t, becomes the sole independent variable in the model. The dependent variables utilized in the model are detailed in Table 1, while the parameters are outlined in Table 2.

Ref. [14] introduced the following dimensionless parameter:

$$\xi = \frac{q_{A,0} L}{D_A} t_f \, k_2 \tag{3}$$

Ref. [14] demonstrated that the lumped capacitance approximation, which assumes that Aβ concentrations depend only on time and not on location within the control volume (CV), holds when $\xi << 1$. In Eq. (3), t_f represents the process duration, and D_A denotes the diffusivity of Aβ monomers. Using a value of 62.3 μm²/s for D_A [19] and taking other parameters from Table 2, ξ is estimated to be 0.026. Therefore, the criterion $\xi << 1$ is met, allowing variations in Aβ monomer concentrations across the CV to be neglected.

By applying the conservation of Aβ monomers within the CV shown in Fig. 1, the following equation is derived:

$$\frac{dC_A}{dt} = -k_1 C_A - k_2 C_A C_B - C_A \frac{\ln(2)}{T_{1/2,A}} + \frac{q_{A,0}}{L} \tag{4}$$

The first term on the right-hand side of Eq. (4) represents the nucleation-driven conversion rate of Aβ monomers into aggregates, while the second term describes the rate of conversion through autocatalytic growth. Additionally, the third term on the right-hand side of Eq. (4) accounts for the degradation of Aβ monomers, and the fourth term simulates the production of Aβ monomers on lipid membranes.

By stating the conservation of free Aβ aggregates within the CV, the following equation is obtained:

$$\frac{dC_B}{dt} = k_1 C_A + k_2 C_A C_B - C_B \frac{\ln(2)}{T_{1/2,B}} - C_B \frac{\ln(2)}{\theta_{1/2,B}} \tag{5}$$

In Eq. (5), the first two terms on the right-hand side are analogous to the first two terms in Eq. (4), but with opposite signs. The third term represents the degradation rate of free Aβ aggregates, while the fourth term models the deposition rate of these aggregates into senile plaques.

The formation of Aβ plaques from adhesive Aβ fibrils is modeled by a method similar to that used for colloidal suspension coagulation [20]. In this model, free Aβ aggregates (*B*) are assumed to deposit into Aβ plaques, and the concentration of these deposited aggregates is denoted as C_D.

$$\frac{dC_D}{dt} = C_B \frac{\ln(2)}{\theta_{1/2,B}} - C_D \frac{\ln(2)}{T_{1/2,D}} \tag{6}$$

In Eq. (6), the first term on the right-hand side corresponds to the fourth term in Eq. (5) but with the opposite sign. The second term reflects the half-life of Aβ aggregates within the senile plaques.

The initial conditions are defined as follows:

$$\text{At } t = 0\text{: } C_A = 0,\ C_B = 0,\ C_D = 0 \tag{7a,b,c}$$

Table 1. Dependent variables utilized in the model.

Symbol	Definition	Units
C_A	Concentration of Aβ monomers	μM
C_B	Concentration of free Aβ aggregates	μM
C_D	Concentration of Aβ aggregates deposited into Aβ plaques	μM

Table 2. Model parameters.

Symbol	Definition	Units	Value or range	Reference or estimation method	Value(s) used in computations
a_{21}	Conversion factor from $\frac{\text{mol}}{\mu\text{m}^3}$ to μM	$\frac{\mu\text{M}\ \mu\text{m}^3}{\text{mol}}$	10^{21}		10^{21}

k_1	Nucleation rate constant for the first pseudo-elementary step in the F-W model	s^{-1}	2.22×10^{-9} [a]	[17,21]	2.22×10^{-9}
k_2	Autocatalytic growth rate constant for the second pseudo-elementary step in the F-W model	$\mu M^{-1}\ s^{-1}$	9.44×10^{-6} [a]	[17,21]	9.44×10^{-6}
L	Half the distance separating senile plaques	μm	50	Estimated from Fig. 1a of [22]	50
MW	Molecular weight of an Aβ monomer, calculated as the total weight of all atoms in the monomer	$g\ mol^{-1}$	4.51×10^{3} [b]	[23]	4.51×10^{3}
$q_{A,0}$	Flux of Aβ monomers through the left boundary of a CV with volume L^3 (Fig. 1)	$\mu M\ \mu m\ s^{-1}$	1.1×10^{-5} [c]	[23]	1.1×10^{-5}
t_f	Duration of senile plaque growth	s	3.15×10^{8} [d]	[24]	3.15×10^{8}
$T_{1/2,A}$	Half-life of Aβ monomers	s	4.61×10^{3} [e]	[19]	4.61×10^{3}, 10^{20} (to represent $T_{1/2,A}\to\infty$)
$T_{1/2,B}$	Half-life of free Aβ aggregates	s	10^{20} [f]		10^{20} (to represent $T_{1/2,B}\to\infty$)

$T_{1/2,D}$	Half-life of Aβ aggregates once they have been deposited into senile plaques	s	10^{20} [f]		10^{20} (to represent $T_{1/2,D} \to \infty$)
ρ	Density of the Aβ plaque	g/μm^3	1.35×10^{-12} [g]	[25]	1.35×10^{-12}
$\theta_{1/2,B}$	Half-deposition time of Aβ aggregates into senile plaques, which is the duration required for half of the aggregates in the suspension to be deposited into the plaque	s	8.64×10^{4} - 1.73×10^{5} [h]	[26,27]	10^{1} (to represent $\theta_{1/2,B} \to 0$), 10^{7}, 10^{20} (to represent $\theta_{1/2,B} \to \infty$)
Ξ_{crit}	Critical value of Ξ above which surrounding neurons die	μM·s	2×10^{9}	See the discussion of Fig. 5	2×10^{9}

[a] The values reported in [17] were derived through curve-fitting of experimental data obtained in [21]. Specifically, the parameters are $k_1 = 8\times10^{-6}$ h^{-1}, $k_2 = 3.4\times10^{-2}$ μM^{-1} h^{-1} [17].

[b] The molecular weight of Aβ42 according to [23].

[c] As reported in [23], the human brain generates Aβ42 monomers at a rate of 0.33×10^{-6} μmol s^{-1}. Given that the brain's approximate volume is 1.5×10^{15} μm^3, the Aβ42 production rate per unit volume is estimated at 2.2×10^{-22} μmol μm^{-3} s^{-1}. Within a small cube of side length L (representing the CV in Fig. 1), the production rate of Aβ42 peptide is calculated to be 2.75×10^{-17} μmol s^{-1}. Aβ monomers are produced at lipid membranes [28]. Assuming that all Aβ42 monomers are released from the left-hand face

of the cube, which has an area of L^2 (Fig. 1), the rate of Aβ42 release per unit area is 1.1×10^{-20} μmol μm^{-2} s^{-1} $=1.1\times10^{-5}$ μM μm s^{-1}.

[d] Holtzman et al. (2011) proposes that the growth period for a senile plaque spans approximately 10 years.

[e] Ref. [19] reports that the half-life of Aβ monomers is approximately 1.28 hours.

[f] In the absence of therapeutic intervention, Aβ aggregates and plaques degrade at a significantly slower rate compared to monomers. Ref. [29] estimates that the turnover of senile plaques occurs over several years. Consequently, for computational purposes, the half-lives of Aβ aggregates and plaques are assumed to be infinite.

[g] A commonly used density value for proteins, irrespective of their specific type, is 1.35 g/cm³ [25].

[h] Several studies have found that individual plaques can develop in a relatively short time frame, ranging from around 24 hours [26] to 48 hours [27].

2.2. Criterion of accumulated toxicity of Aβ oligomers

The exact mechanism behind the toxicity of Aβ oligomers is not well understood. Certain Aβ oligomers may be more toxic than others. Alternatively, a mixture of different oligomers with varying structures, stability, and concentrations might cause nonspecific toxicity by binding to membrane proteins, targeting membrane lipids, inducing oxidative stress, and altering membrane dielectric properties and ion permeability [10]. If an "Aβ soup" is responsible for nonspecific toxicity, the parameter characterizing the accumulated toxicity of Aβ is

$$\Xi(t)=\int_0^t C_B(\hat{t})\,d\hat{t} \tag{8}$$

The dimensionless version of Eqs. (4)-(8) is given in section S1.1 of the Supplementary Materials.

If toxicity is caused by several specific toxic oligomer species, the criterion for toxicity can be redefined as follows (for example):

$$\Xi(t)=\int_0^t C_{B,1}(\hat{t})\,d\hat{t}+\int_0^t C_{B,2}(\hat{t})\,d\hat{t}+\ldots \tag{9}$$

2.3. A model for senile plaque growth

A methodology developed in [14] is followed. To simulate the growth of an Aβ plaque (illustrated in Fig. 1), the approach involves determining the total number of Aβ monomers, represented by *N*, that have been incorporated into the plaque over time *t*. This can be done by using the average concentration of Aβ monomers deposited into the plaque, as suggested in [30]:

$$N(t) = 2N_A \frac{L^3}{a_{21}} C_D(t) \tag{10}$$

where the coefficient of 2 arises from the model's assumption that the Aβ plaque forms between two adjacent neurons. Each neuron's membrane releases Aβ monomers at a rate of $q_{A,0}$, contributing to the plaque's development (Fig. 1).

Another approach, which also follows [30], is determining $N(t)$ through the volume of a single inclusion body, V_{ABP}:

$$N(t) = N_A \frac{V_{ABP}(t)\rho}{MW} \tag{11}$$

where MW denotes the average molecular weight of an Aβ monomer.

By equating the right-hand sides of Eqs. (10) and (11) and solving for the volume of the Aβ plaque, the following expression is derived:

$$V_{ABP}(t) = 2\frac{MW}{\rho}\frac{L^3}{a_{21}} C_D(t) \tag{12}$$

where $a_{21} = 10^{21} \frac{\mu\text{M}\ \mu\text{m}^3}{\text{mol}}$ is the conversion factor from $\frac{\text{mol}}{\mu\text{m}^3}$ to μM.

Assuming the Aβ plaque takes on a spherical shape,

$$V_{ABP}(t) = \frac{4\pi}{3} r_{ABP}^3(t) \tag{13}$$

By equating the right sides of Eqs. (12) and (13) and solving for the radius of the Aβ plaque, the following expression is derived:

$$r_{ABP} = \left(\frac{3}{2\pi}\frac{MW}{\rho}\frac{L^3}{a_{21}} C_D(t) \right)^{1/3} \tag{14}$$

3. Analytical solutions for the limiting cases

3.1. The scenario of a slow deposition rate of Aβ aggregates into senile plaques, $\theta_{1/2,B} \to \infty$, as well as $T_{1/2,A} \to \infty$ and $T_{1/2,B} \to \infty$

For a slow deposition rate of Aβ aggregates into senile plaques and infinitely large half-lives of monomers and free aggregates, Eqs. (4)-(6) reduce to, respectively,

$$\frac{dC_A}{dt} = -k_1 C_A - k_2 C_A C_B + \frac{q_{A,0}}{L} \tag{15}$$

$$\frac{dC_B}{dt} = k_1 C_A + k_2 C_A C_B \tag{16}$$

$$C_D = 0 \tag{17}$$

Eqs. (15) and (16) were solved using the initial conditions (7a,b), as detailed in [14,31]. For completeness, the analytical solutions to Eqs. (15) and (16) are provided in section S1.2 of the Supplementary Materials.

The exact solution given by Eqs. (S10) and (S12) is rather cumbersome. A more elegant approximate solution is

$$C_A = \frac{\frac{q_{A,0}}{L}}{k_1 + k_2 \frac{q_{A,0}}{L} t} \tag{18}$$

$$C_B = \frac{q_{A,0}}{L} t \tag{19}$$

Note that as $t \to \infty$, Eq. (18) leads to $C_A \to 0$.

Using Eqs. (8) and (19),

$$\Xi(t) = \frac{q_{A,0}}{L} \frac{t^2}{2} \tag{20}$$

The quadratic dependence on time indicates that initially the accumulated toxicity grows slowly, but as time progresses, it increases more rapidly.

3.2. The scenario of a fast deposition rate of Aβ aggregates into senile plaques, $\theta_{1/2,B} \to 0$, as well as $T_{1/2,A} \to \infty$ and $T_{1/2,B} \to \infty$

As $\theta_{1/2,B} \to 0$, which means immediate deposition of Aβ aggregates into plaques, Eqs. (4)-(6) simplify to, respectively,

$$C_B = 0 \tag{21}$$

$$\frac{dC_A}{dt} = -k_1 C_A + \frac{q_{A,0}}{L} \tag{22}$$

$$\frac{dC_D}{dt} = k_1 C_A \tag{23}$$

In this case, Eqs. (8) and (21) lead to

$$\Xi(t) = 0 \tag{24}$$

Adding Eqs. (22) and (23) gives

$$\frac{dC_A}{dt} + \frac{dC_D}{dt} = \frac{q_{A,0}}{L} \tag{25}$$

Integrating Eq. (25) over time and applying the initial conditions from Eq. (7a,c), the following result is derived:

$$C_A + C_D = \frac{q_{A,0}}{L} t \tag{26}$$

The increase in $C_A + C_D$ over time is due to the influx of newly synthesized Aβ monomers at the left boundary of the CV. By substituting C_A from Eq. (26) into Eq. (23), the following is derived:

$$\frac{dC_D}{dt} = k_1 \left(\frac{q_{A,0}}{L} t - C_D \right) \tag{27}$$

The exact solution of Eq. (27) with the initial condition specified in Eq. (7c) is

$$C_D = \frac{q_{A,0}}{k_1 L} \left(-1 + e^{-k_1 t} + k_1 t \right) \tag{28}$$

As $t \to 0$, Eq. (28) becomes

$$C_D \to \frac{k_1 q_{A,0} t^2}{2L} \tag{29}$$

indicating that at small *t*, the concentration of Aβ aggregates deposited into Aβ plaques is directly proportional to the kinetic constant characterizing the nucleation of Aβ aggregates.

The quantity C_A can then be determined using Eqs. (26) and (28) as

$$C_A = \frac{q_{A,0}}{L} t - \frac{q_{A,0}}{k_1 L}\left(-1 + e^{-k_1 t} + k_1 t\right) \tag{30}$$

4. Sensitivity analysis

One of the primary objectives of this study was to examine the sensitivity of accumulated toxicity, Ξ, in response to various parameters.

This involved calculating the local sensitivity coefficients, which are the first-order partial derivatives of the observable (the accumulated toxicity) with respect to parameters such as the nucleation rate constant for the first pseudo-elementary step in the F-W model, k_1. This analysis followed the methodology outlined in [32-35]. Specifically, the sensitivity coefficient of Ξ to a parameter (for example) k_1 was determined using

$$\frac{\partial \Xi}{\partial k_1} \approx \left.\frac{\Xi\left(k_1 + \Delta k_1\right) - \Xi\left(k_1\right)}{\Delta k_1}\right|_{\text{other parmeters kept constant}} \tag{31}$$

where $\Delta k_1 = 10^{-3} k_1$ is the step size. Calculations were conducted with various step sizes to evaluate the sensitivity coefficients' independence from the step size.

The non-dimensional relative sensitivity coefficients were computed following the method described in [33,36], for example,

$$S_{k_1}^{\Xi} = \frac{k_1}{\Xi}\frac{\partial \Xi}{\partial k_1} \tag{32}$$

From Eq. (20), the following is obtained:

$$S_{k_1}^{\Xi} = 0 \tag{33}$$

$$S_{k_2}^{\Xi} = 0 \tag{34}$$

$$S_{q_{A,0}}^{\Xi} = 1 \tag{35}$$

$$S_{t}^{\Xi} = 2 \tag{36}$$

$$S_{L}^{\Xi} = -1 \tag{37}$$

5. Results

Details of the numerical solution methodology are provided in Section S1.3 of the Supplementary Materials.

Figs. S1 and S2 display the concentrations of Aβ monomers, $C_A(t)$, free Aβ aggregates, $C_B(t)$, Aβ aggregates deposited in plaques, $C_D(t)$, and the radius of a growing Aβ plaque, $r_{ABP}(t)$, for different values of k_1. Interestingly, C_A appears to be independent of k_1 (Fig. S1a). Indeed, in this scenario, the last two terms in Eq. (3) are dominant. By equating these terms, the following estimate of C_A is derived:

$$C_A = \frac{q_{A,0}}{L}\frac{T_{1/2,A}}{\ln(2)} = 1.5\times10^{-3}\ \mu\text{M} \tag{38}$$

This corresponds to the value that C_A rapidly reaches in Fig. S1a. Note that the value derived from Eq. (38) is independent of k_1.

The value that C_B reaches in Fig. S1b depends on k_1 because the production rate of free aggregates through nucleation, $k_1 C_A$, is directly proportional to k_1 (refer to Eq. (5)).

Since free aggregates deposit into plaques (see Eq. (6)), an increase in k_1 also leads to a rise in the concentration of deposited aggregates, C_D (Fig. S2a). Notably, C_D increases linearly over time (Fig. 2a). This can be attributed to the assumed constant rate of Aβ monomer production, $q_{A,0}$, and the fact that the rate of Aβ monomer degradation, $C_A \frac{\ln(2)}{T_{1/2,A}}$, remains unaffected by k_1 in this scenario.

Since the radius of the plaque is proportional to the cube root of the concentration of deposited aggregates (see Eq. (14)), $C_D(t)$ increases in proportion to $t^{1/3}$. Consequently, the increase in k_1 also leads to an increase in C_D (Fig. 2b).

Figs. S3 and S4 display $C_A(t)$, $C_B(t)$, $C_D(t)$, and $r_{ABP}(t)$ for various values of k_2. The dependence of $C_A(t)$ on *t* becomes more complex; for the greatest value of k_2 the monomer concentration decreases as *t* increases. This occurs because k_2 controls the production of free Aβ aggregates from monomers via autocatalytic growth, represented by the nonlinear term, $k_2 C_A C_B$, in Eq. (4). This nonlinear process cannot be easily balanced by the linear term governing Aβ monomer degradation, $C_A \frac{\ln(2)}{T_{1/2,A}}$, in Eq. (4). The values of C_B, C_D, and r_{ABP} increase as k_2 increases, but now in a nonlinear manner, increasing much faster for larger values of k_2 (Figs. S3a, S4a, and S4b).

Figs. S5 and S6 display $C_A(t)$, $C_B(t)$, $C_D(t)$, and $r_{ABP}(t)$ for different values of $q_{A,0}$. The behavior of these quantities with respect to $q_{A,0}$ is somewhat similar to its dependence on k_2; $C_A(t)$ decreases with *t* for large values of $q_{A,0}$ (Fig. S5a). Meanwhile, C_B, C_D, and r_{ABP} increase as $q_{A,0}$ increases, with this growth accelerating significantly for greater values of $q_{A,0}$.

In Fig. 2a, the accumulated toxicity, Ξ, increases quadratically over time. For $\theta_{1/2,B} = 10^7$ s, the increase in k_1 leads to a corresponding increase in Ξ (Fig. 2a). The increase remains slow when k_1 is small but accelerates as k_1 increases. As $\theta_{1/2,B} \to \infty$, Ξ becomes independent of k_1 and aligns with the analytical solution given by Eq. (20) (Fig. 2b). It is important to note that the analytical solution predicts that $\Xi \sim t^2$.

At low values of k_2, the accumulated toxicity, Ξ, remains small but increases rapidly when k_2 becomes large (Fig. 3a). In the case where $\theta_{1/2,B} \to \infty$, Ξ becomes independent of k_2 and coincides with the analytical result from Eq. (20) (Fig. 3b).

When $q_{A,0}$ is small, the accumulated toxicity, Ξ, stays low but surges dramatically as $q_{A,0}$ increases to its maximum value in Fig. 4a. As $\theta_{1/2,B} \to \infty$, Ξ aligns with the analytical prediction from Eq. (20). In this scenario, Ξ exhibits a linear dependence on $q_{A,0}$ (see Eq. (20)), explaining the different lines observed for different values of $q_{A,0}$ in Fig. 4b.

The results shown in Fig. 4a, illustrating $\Xi(t)$, and Fig. S6b, depicting $r_{ABP}(t)$, have been combined to create Fig. 5, which shows $\Xi = f(r_{ABP})$. Despite recent criticisms of the amyloid hypothesis in Alzheimer's disease (AD) by some authors [37,38], many researchers still believe there is a strong correlation between the accumulation of sticky amyloid proteins in the brain and AD [39]. Assuming the largest plaque sizes correspond to the most advanced stages of the disease and that nearby neurons die when plaques reach a significant size, the threshold value for Ξ can be estimated from Fig. 5 at approximately 2×10^9 μM·s.

As $\theta_{1/2,B} \to 0$, free aggregates immediately deposit into plaques, leading to $\Xi \to 0$. The question arises as to what happens with Ξ when $\theta_{1/2,B}$ is increased. This issue is explored in Figs. 6-8. For a finite half-life of Aβ monomers, $T_{1/2,A}$, the accumulated toxicity exhibits a rapid S-shaped increase around $\theta_{1/2,B} \approx 10^7$ s and then it plateaus, reaching a level still lower than the analytical prediction in Eq. (20) (Fig. 6a). However, as $T_{1/2,A} \to \infty$, Ξ reaches the value predicted by the analytical solution at higher $\theta_{1/2,B}$ values (Fig. 6b). For finite $T_{1/2,A}$, the numerical curves differ for various k_1, but as $T_{1/2,A} \to \infty$, the curves converge (compare Fig. 6a and 6b). Notably, some curves in Fig. 6 cross the solid black horizontal line, which represents the critical value of Ξ, 2×10^9 μM·s. This indicates that in the simulated CV, the accumulated toxicity exceeds its critical value, resulting in the death of nearby neurons.

Figs. 7a and 7b, which show accumulated toxicity as a function of $\theta_{1/2,B}$ for various values of k_2, tell a similar story. When $T_{1/2,A}$ is finite (Fig. 7a), the $\Xi = f(\theta_{1/2,B})$ curves differ for different k_2, but as $T_{1/2,A} \to \infty$ (Fig. 7b), the curves converge. As $\theta_{1/2,B}$ increases, some of these curves surpass the critical threshold of Ξ, 2×10^9 μM·s, indicating that nearby neurons are likely to die.

Figs. 8a and 8b illustrate how the curves for $\Xi = f(\theta_{1/2,B})$ vary with $q_{A,0}$. Notably, the analytical solution given by Eq. (20) depends on $q_{A,0}$, so each value of $q_{A,0}$ corresponds to a different line in Figs. 8a and 8b. In Fig. 8b, which depicts the scenario where $T_{1/2,A} \to \infty$, each line for a different $q_{A,0}$ approaches its own asymptotic limit, matching the value predicted by the analytical solution as $\theta_{1/2,B} \to \infty$.

The sensitivity of accumulated toxicity, Ξ, to the nucleation rate constant, k_1, is positive (Fig. 9a). This indicates that increasing k_1 results in a corresponding increase in Ξ. This aligns with the trend observed

in Fig. 2a. From Fig. 9b, it is evident that in the scenario where $T_{1/2,A} \to \infty$ and $\theta_{1/2,B} \to \infty$, $S_{k_1}^{\Xi}$ approaches the analytically predicted value of zero over time (see Eq. (33)).

Accumulated toxicity, Ξ, exhibits a positive sensitivity to the rate constant describing autocatalytic growth, k_2 (Fig. 10a), so a greater k_2 leads to an increase in Ξ. This trend is consistent with the result depicted in Fig. 3a. As shown in Fig. 10b, as $T_{1/2,A} \to \infty$ and $\theta_{1/2,B} \to \infty$, $S_{k_2}^{\Xi}$ converges to the zero value predicted by the analytical solution as time progresses (see Eq. (34)).

The sensitivity of accumulated toxicity, Ξ, to the flux of Aβ monomers, $q_{A,0}$, is also positive (Fig. 11a). Hence, increasing $q_{A,0}$ leads to a higher Ξ. This result aligns with the observation in Fig. 4a. Fig. 11b shows that as $T_{1/2,A} \to \infty$ and $\theta_{1/2,B} \to \infty$, $S_{q_{A,0}}^{\Xi}$ reaches the analytically predicted value of unity as time increases (see Eq. (35)).

6. Discussion, limitations of the model, and future directions

A criterion for characterizing the accumulated toxicity of Aβ oligomers is developed, and a critical threshold is proposed, beyond which nearby neurons are expected to die. If Aβ monomers and aggregates have an infinite half-life, then accumulated toxicity, Ξ, shows an S-shaped growth pattern as the half-deposition time of Aβ aggregates into senile plaques, $\theta_{1/2,B}$, increases. Once $\theta_{1/2,B}$ becomes sufficiently large, Ξ levels off and aligns with the value predicted by the analytical solution for Ξ.

The analytical solution in Eq. (20), which is valid for a small rate of deposition of free aggregates into senile plaques (large $\theta_{1/2,B}$) and an infinitely long half-life of Aβ monomers and aggregates, indicates that accumulated toxicity is proportional to the square of the duration of the senile plaque formation process. This implies that, given enough time (assuming a long enough lifespan), the accumulated toxicity will eventually surpass the critical threshold, leading to neuron death. However, the analytical solution is only valid in the scenario of infinitely long half-life of Aβ monomers and free aggregates, indicating a malfunctioning degradation machinery for both monomers and aggregates. Therefore, the model suggests that if the protein degradation machinery is impaired, AD becomes inevitable—it is only a matter of time before neurons begin to die. The only way to prevent this is by ensuring that the degradation machinery for Aβ remains functional. This aligns with a hypothesis proposed by several researchers, suggesting that an imbalance between Aβ production and clearance can lead to accumulation of misfolded Aβ in the brain [40].

The quadratic dependence on the duration of the process predicted by the analytical solution (Eq. (20)) suggests that the toxicity accumulation starts off slowly but accelerates over time. This may explain why AD symptoms take so long to manifest.

Accumulated toxicity, Ξ, exhibits positive sensitivity to the nucleation rate constant, k_1, the autocatalytic growth rate constant, k_2, and the flux of Aβ monomers, $q_{A,0}$. For each of these cases, the sensitivity converges to the analytically predicted values when the half-deposition time of Aβ aggregates into senile plaques, $\theta_{1/2,B}$, is large, and when the half-lives for Aβ monomers and aggregates, $T_{1/2,A}$ and $T_{1/2,B}$, respectively, are infinitely long.

The toxicity of Aβ plaques might be attributed to the high concentration of oligomers accumulating near the plaques due to their deposition. To test this hypothesis, it would be beneficial to develop a model that quantifies oligomer concentration in the diffusion boundary layer near a plaque's surface. This model could also assess the likelihood that these elevated oligomer levels could trigger inflammatory responses, resulting in neuronal damage. Additionally, developing a model to simulate the interactions between a diverse array of oligomers and cellular membranes would be valuable.

The F-W model lumps all aggregates, such as dimers and trimers, into a single phase representing all free amyloid-converted peptides (phase *B* in Eqs. (1) and (2)) with a concentration denoted as C_B. As a result, it does not differentiate between various types of Aβ oligomers. Future research should address this limitation by using more detailed models that can simulate the formation of different Aβ oligomers.

It would be also important to establish a correlation between the criterion developed in this paper and the severity of cognitive decline in patients. A significant next step in this research would be to develop a criterion that accounts for the combined neural damage caused by Aβ oligomers and pathological tau.

Data accessibility. This article has no additional data.

Authors' contributions. AVK is the sole author of this paper.

Competing interests. The author declares no competing interests.

Funding statement. The author acknowledges the support provided by the National Science Foundation (grant CBET-2042834) and the Alexander von Humboldt Foundation through the Humboldt Research Award.

References

1. Hardy J. 2006 A hundred years of Alzheimer's disease research. *Neuron* **52,** 3-13. (doi:10.1016/j.neuron.2006.09.016)

2. Maqbool M, Mobashir M, Hoda N. 2016 Pivotal role of glycogen synthase kinase-3: A therapeutic target for Alzheimer's disease. *Eur. J. Med. Chem.* **107,** 63-81. (doi:10.1016/j.ejmech.2015.10.018)

3. Hung S, Fu W. 2017 Drug candidates in clinical trials for Alzheimer's disease. *J. Biomed. Sci.* **24,** 47. (doi:10.1186/s12929-017-0355-7)

4. Knopman DS, Amieva H, Petersen RC, Chételat G, Holtzman DM, Hyman BT, Nixon RA, Jones DT. 2021 Alzheimer disease. *Nature Reviews Disease Primers* **7,** 33. (doi:10.1038/s41572-021-00269-y)

5. Breijyeh Z, Karaman R. 2020 Comprehensive review on Alzheimer's disease: Causes and treatment. *Molecules* **25,** 5789. doi: 10.3390/molecules25245789. (doi:10.3390/molecules25245789)

6. Thacker D, Barghouth M, Bless M, Zhang E, Linse S. 2023 Direct observation of secondary nucleation along the fibril surface of the amyloid β 42 peptide. *Proceedings of the National Academy of Sciences* **120,** e2220664120. (doi:10.1073/pnas.2220664120)

7. O'Brien RJ, Wong PC. 2011 Amyloid precursor protein processing and Alzheimer's disease. *Annual Review of Neuroscience* **34,** 185-204. (doi:10.1146/annurev-neuro-061010-113613)

8. Hampel H, Hardy J, Blennow K, Chen C, Perry G, Kim SH, Villemagne VL, Aisen P, Vendruscolo M, Iwatsubo T, Masters CL, Cho M, Lannfelt L, Cummings JL, Vergallo A. 2021 The amyloid-β pathway in Alzheimer's disease. *Mol. Psychiatry* **26,** 5481-5503. (doi:10.1038/s41380-021-01249-0)

9. Rahman MM, Lendel C. 2021 Extracellular protein components of amyloid plaques and their roles in Alzheimer's disease pathology. *Molecular Neurodegeneration* **16,** 59. (doi:10.1186/s13024-021-00465-0)

10. Benilova I, Karran E, De Strooper B. 2012 The toxic aβ oligomer and Alzheimer's disease: An emperor in need of clothes. *Nat. Neurosci.* **15,** 349-357. (doi:10.1038/nn.3028)

11. Ono K, Condron MM, Teplow DB. 2009 Structure–neurotoxicity relationships of amyloid β-protein oligomers. *Proceedings of the National Academy of Sciences* **106,** 14745-14750. (doi:10.1073/pnas.0905127106)

12. Mrdenovic D, Pieta IS, Nowakowski R, Kutner W, Lipkowski J, Pieta P. 2022 Amyloid β interaction with model cell membranes – what are the toxicity-defining properties of amyloid β? *Int. J. Biol. Macromol.* **200,** 520-531. (doi:10.1016/j.ijbiomac.2022.01.117)

13. Kuznetsov AV. 2023 Effect of diffusivity of amyloid beta monomers on the formation of senile plaques. *bioRxiv* 2023.07.31.551367. (doi:10.1101/2023.07.31.551367)

14. Kuznetsov AV. 2024 Numerical and analytical simulation of the growth of amyloid-β plaques. *ASME Journal of Biomedical Engineering* **146,** 061004. (doi:10.1115/1.4064969)

15. Kuznetsov AV. 2024 Numerical modeling of senile plaque development under conditions of limited diffusivity of amyloid-β monomers. *Journal of Theoretical Biology* **587,** 111823. (doi:10.1101/2024.01.09.574935)

16. Kuznetsov AV. 2024 The growth rate of senile plaques is determined by the competition between the rate of deposition of free aβ aggregates into plaques and the autocatalytic production of free aβ aggregates. *Journal of Theoretical Biology* **593,** 111900. (doi:10.1016/j.jtbi.2024.111900)

17. Morris AM, Watzky MA, Agar JN, Finke RG. 2008 Fitting neurological protein aggregation kinetic data via a 2-step, minimal/"Ockham's razor" model: The Finke-Watzky mechanism of nucleation followed by autocatalytic surface growth. *Biochemistry* **47,** 2413-2427. (doi:10.1021/bi701899y)

18. Iashchishyn IA, Sulskis D, Nguyen Ngoc M, Smirnovas V, Morozova-Roche LA. 2017 Finke-Watzky two-step nucleation-autocatalysis model of S100A9 amyloid formation: Protein misfolding as "nucleation" event. *ACS Chem. Neurosci.* **8,** 2152-2158. (doi:10.1021/acschemneuro.7b00251)

19. Waters J. 2010 The concentration of soluble extracellular amyloid-beta protein in acute brain slices from CRND8 mice. *PLOS One* **5,** e15709. (doi:10.1371/journal.pone.0015709)

20. Boltachev GS, Ivanov MG. 2020 Effect of nanoparticle concentration on coagulation rate of colloidal suspensions. *Heliyon* **6,** e03295. (doi:10.1016/j.heliyon.2020.e03295)

21. Bieschke J, Zhang Q, Powers ET, Lerner RA, Kelly JW. 2005 Oxidative metabolites accelerate Alzheimer's amyloidogenesis by a two-step mechanism, eliminating the requirement for nucleation. *Biochemistry* **44,** 4977-4983. (doi:10.1021/bi0501030)

22. Querol-Vilaseca M, Colom-Cadena M, Pegueroles J, Nuñez-Llaves R, Luque-Cabecerans J, Muñoz-Llahuna L, Andilla J, Belbin O, Spires-Jones T, Gelpi E, Clarimon J, Loza-Alvarez P, Fortea J, Lleó A. 2019 Nanoscale structure of amyloid-β plaques in Alzheimer's disease. *Scientific Reports* **9,** 5181. (doi:10.1038/s41598-019-41443-3)

23. Raskatov JA. 2019 What is the "Relevant" amyloid β42 concentration? *ChemBioChem* **20,** 1725-1726. (doi:10.1002/cbic.201900097)

24. Holtzman DM, Morris JC, Goate AM. 2011 Alzheimer's disease: The challenge of the second century. *Science Translational Medicine* **3,** 77sr1. (doi:10.1126/scitranslmed.3002369)

25. Cavicchi RE, King J, Ripple DC. 2018 Measurement of average aggregate density by sedimentation and brownian motion analysis. *J. Pharm. Sci.* **107,** 1304-1312. (doi:10.1016/j.xphs.2018.01.013)

26. Meyer-Luehmann M, Spires-Jones TL, Prada C, Garcia-Alloza M, de Calignon A, Rozkalne A, Koenigsknecht-Talboo J, Holtzman DM, Bacskai BJ, Hyman BT. 2008 Rapid appearance and local toxicity of amyloid-beta plaques in a mouse model of Alzheimer's disease. *Nature* **451,** 720-724. (doi:10.1038/nature06616)

27. Han S, Kollmer M, Markx D, Claus S, Walther P, Fändrich M. 2017 Amyloid plaque structure and cell surface interactions of β-amyloid fibrils revealed by electron tomography. *Scientific Reports* **7,** 43577. (doi:10.1038/srep43577)

28. Dawkins E, Derks RJE, Schifferer M, Trambauer J, Winkler E, Simons M, Paquet D, Giera M, Kamp F, Steiner H. 2023 Membrane lipid remodeling modulates γ-secretase processivity. *J. Biol. Chem.* **299,** 103027. (doi:10.1016/j.jbc.2023.103027)

29. Madrasi K, Das R, Mohmmadabdul H, Lin L, Hyman BT, Lauffenburger DA, Albers MW, Rissman RA, Burke JM, Apgar JF, Wille L, Gruenbaum L, Hua F. 2021 Systematic in silico analysis of clinically tested drugs for reducing amyloid-beta plaque accumulation in Alzheimer's disease. *Alzheimer's Dement.* **17,** 1487-1498. (doi:10.1002/alz.12312)

30. Watzky MA, Finney EE, Finke RG. 2008 Transition-metal nanocluster size vs formation time and the catalytically effective nucleus number: A mechanism-based treatment. *J. Am. Chem. Soc.* **130,** 11959-11969. (doi:10.1021/ja8017412)

31. Kuznetsov IA, Kuznetsov AV. 2022 An analytical solution simulating growth of Lewy bodies. *Math. Med. Biol.* **39,** 299-312. (doi:10.1093/imammb/dqac006)

32. Beck JV, Arnold KJ. 1977 *Parameter Estimation in Science and Engineering.* New York: Wiley.

33. Zadeh KS, Montas HJ. 2010 A class of exact solutions for biomacromolecule diffusion-reaction in live cells. *J. Theor. Biol.* **264,** 914-933. (doi:10.1016/j.jtbi.2010.03.028)

34. Zi Z. 2011 Sensitivity analysis approaches applied to systems biology models. *IET Systems Biology* **5,** 336-346. (doi:10.1049/iet-syb.2011.0015)

35. Kuznetsov IA, Kuznetsov AV. 2019 Investigating sensitivity coefficients characterizing the response of a model of tau protein transport in an axon to model parameters. *Comput. Methods Biomech. Biomed. Engin.* **22,** 71-83. (doi:10.1080/10255842.2018.1534233)

36. Kacser H, Burns JA, Fell DA. 1995 The control of flux. *Biochem. Soc. Trans.* **23,** 341-366. (doi:10.1042/bst0230341)

37. Herrup K. 2015 The case for rejecting the amyloid cascade hypothesis. *Nat. Neurosci.* **18,** 794-799. (doi:10.1038/nn.4017)

38. Ricciarelli R, Fedele E. 2017 The amyloid cascade hypothesis in Alzheimer's disease: It's time to change our mind. *Curr. Neuropharmacol.* **15,** 926-935. (doi:10.2174/1570159X15666170116143743)

39. Reardon S. 2023 The brain cells linked to protection against dementia. *Nature* **622,** 229-230. (doi:10.1038/d41586-023-03012-7)

40. Wang W, Hou T, Jia L, Wu Q, Quan M, Jia J. 2019 Toxic amyloid-β oligomers induced self-replication in astrocytes triggering neuronal injury. *EBioMedicine* **42,** 174-187. (doi:10.1016/j.ebiom.2019.03.049)

Figure captions

Fig. 1. A CV with side length L is used to simulate the aggregation of Aβ monomers into free aggregates and their subsequent deposition into senile plaques. Aβ monomers are assumed to be produced at the x=0 boundary. The boundary at x=L is treated as symmetric, preventing any flux of Aβ monomers. The formation of an Aβ plaque is assumed to occur at the symmetric interface between two adjacent CVs. A lumped capacitance approximation is employed, allowing the assumption that all Aβ concentrations are functions of time only.

Fig. 2. Accumulated toxicity of Aβ oligomers, Ξ, as a function of time (in years). Results are shown for three different values of k_1. (a) $T_{1/2,A} = 4.61\times10^3$ and $\theta_{1/2,B} = 10^7$ s, (b) $T_{1/2,A} \to \infty$ and $\theta_{1/2,B} \to \infty$. Note that as $\theta_{1/2,B} \to 0$, all free aggregates immediately deposit into plaques, resulting in $\Xi \to 0$.

Fig. 3. Accumulated toxicity of Aβ oligomers, Ξ, as a function of time (in years). Results are shown for three different values of k_2. (a) $T_{1/2,A} = 4.61\times10^3$ s and $\theta_{1/2,B} = 10^7$ s, (b) $T_{1/2,A} \to \infty$ and $\theta_{1/2,B} \to \infty$. Note that as $\theta_{1/2,B} \to 0$, all free aggregates immediately deposit into plaques, resulting in $\Xi \to 0$.

Fig. 4. Accumulated toxicity of Aβ oligomers, Ξ, as a function of time (in years). Results are shown for three different values of $q_{A,0}$. (a) $T_{1/2,A} = 4.61\times10^3$ s and $\theta_{1/2,B} = 10^7$ s, (b) $T_{1/2,A} \to \infty$ and $\theta_{1/2,B} \to \infty$. Note that as $\theta_{1/2,B} \to 0$, all free aggregates immediately deposit into plaques, resulting in $\Xi \to 0$.

Fig. 5. Accumulated toxicity of Aβ oligomers, Ξ, as a function of the radius of a growing Aβ plaque, r_{ABP}. Results are shown for three different values of $q_{A,0}$. The depicted scenario assumes a finite half-life of Aβ monomers ($T_{1/2,A} = 4.61\times10^3$ s) and an intermediate value of half-deposition time for Aβ aggregates into senile plaques ($\theta_{1/2,B} = 10^7$ s).

Fig. 6. Accumulated toxicity of Aβ oligomers, Ξ, as a function of the half-deposition time of Aβ aggregates into senile plaques, $\theta_{1/2,B}$. Results are presented at $t = t_f = 3.15\times10^8$ s for three different values of k_1. (a) $T_{1/2,A} = 4.61\times10^3$ s, (b) $T_{1/2,A} \to \infty$. Note that as $T_{1/2,A} \to \infty$ all free aggregates immediately deposit into plaques, resulting in $\Xi \to 0$.

Fig. 7. Accumulated toxicity of Aβ oligomers, Ξ, as a function of the half-deposition time of Aβ aggregates into senile plaques, $\theta_{1/2,B}$. Results are presented at $t = t_f = 3.15\times10^8$ s for three different

values of k_2. (a) $T_{1/2,A} = 4.61 \times 10^3$ s, (b) $T_{1/2,A} \to \infty$. Note that as $T_{1/2,A} \to \infty$ all free aggregates immediately deposit into plaques, resulting in $\Xi \to 0$.

Fig. 8. Accumulated toxicity of Aβ oligomers, Ξ, as a function of the half-deposition time of Aβ aggregates into senile plaques, $\theta_{1/2,B}$. Results are presented at $t = t_f = 3.15 \times 10^8$ s for three different values of $q_{A,0}$. (a) $T_{1/2,A} = 4.61 \times 10^3$ s, (b) $T_{1/2,A} \to \infty$. Note that as $T_{1/2,A} \to \infty$ all free aggregates immediately deposit into plaques, resulting in $\Xi \to 0$.

Fig. 9. Sensitivity of the accumulated toxicity, Ξ, to the rate constant that describes the nucleation of Aβ aggregates, k_1. Results are shown for three different values of k_1. (a) $T_{1/2,A} = 4.61 \times 10^3$ s and $\theta_{1/2,B} = 10^7$ s, (b) $T_{1/2,A} \to \infty$ and $\theta_{1/2,B} \to \infty$.

Fig. 10. Sensitivity of the accumulated toxicity, Ξ, to the rate constant that describes the autocatalytic growth Aβ aggregates, k_2. Results are shown for three different values of k_2. (a) $T_{1/2,A} = 4.61 \times 10^3$ s and $\theta_{1/2,B} = 10^7$ s, (b) $T_{1/2,A} \to \infty$ and $\theta_{1/2,B} \to \infty$.

Fig. 11. Sensitivity of the accumulated toxicity, Ξ, to the flux of Aβ monomers, $q_{A,0}$. Results are shown for three different values of $q_{A,0}$. (a) $T_{1/2,A} = 4.61 \times 10^3$ s and $\theta_{1/2,B} = 10^7$ s, (b) $T_{1/2,A} \to \infty$ and $\theta_{1/2,B} \to \infty$.

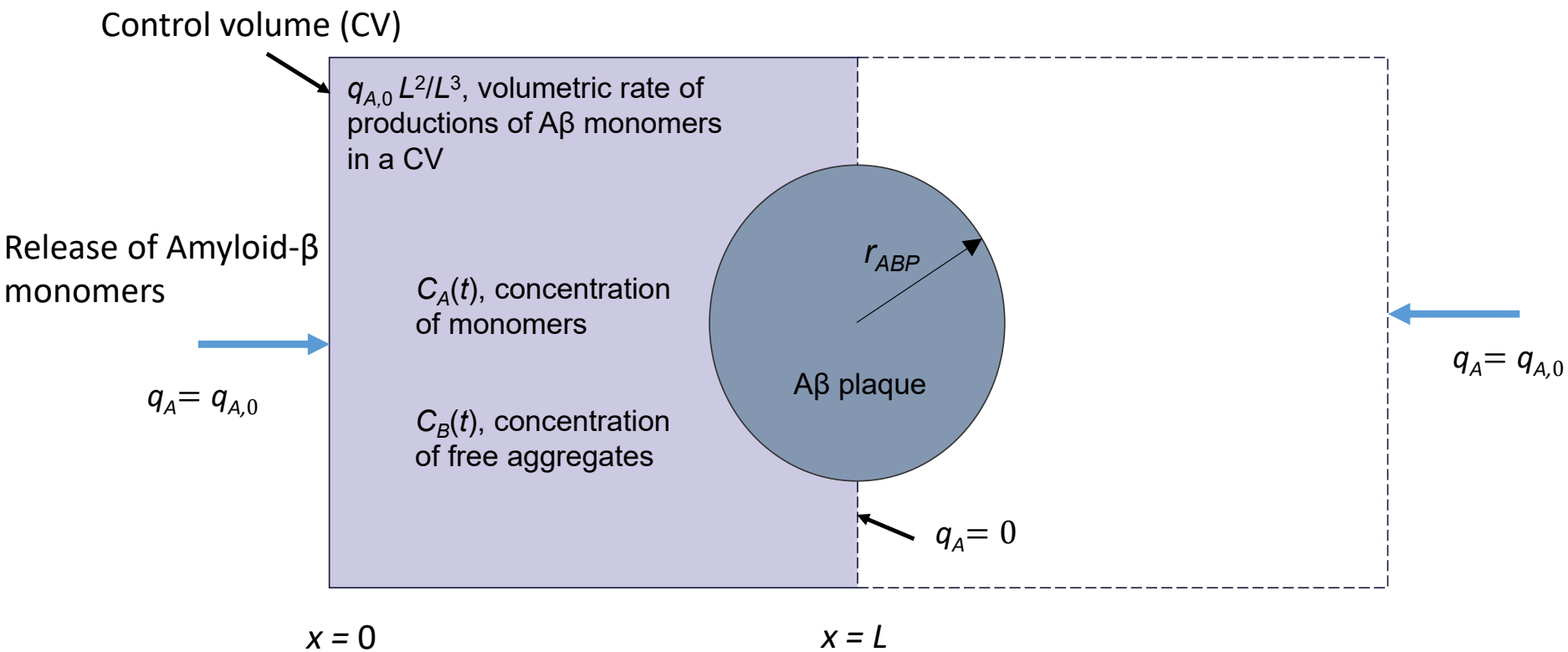
Control volume (CV)
$q_{A,0}\,L^2/L^3$, volumetric rate of productions of Aβ monomers in a CV
Release of Amyloid-β monomers
$C_A(t)$, concentration of monomers
$C_B(t)$, concentration of free aggregates
r_{ABP}
Aβ plaque
$q_A = q_{A,0}$
$q_A = q_{A,0}$
$q_A = 0$
$x = 0$
$x = L$

Figure 1

(a)

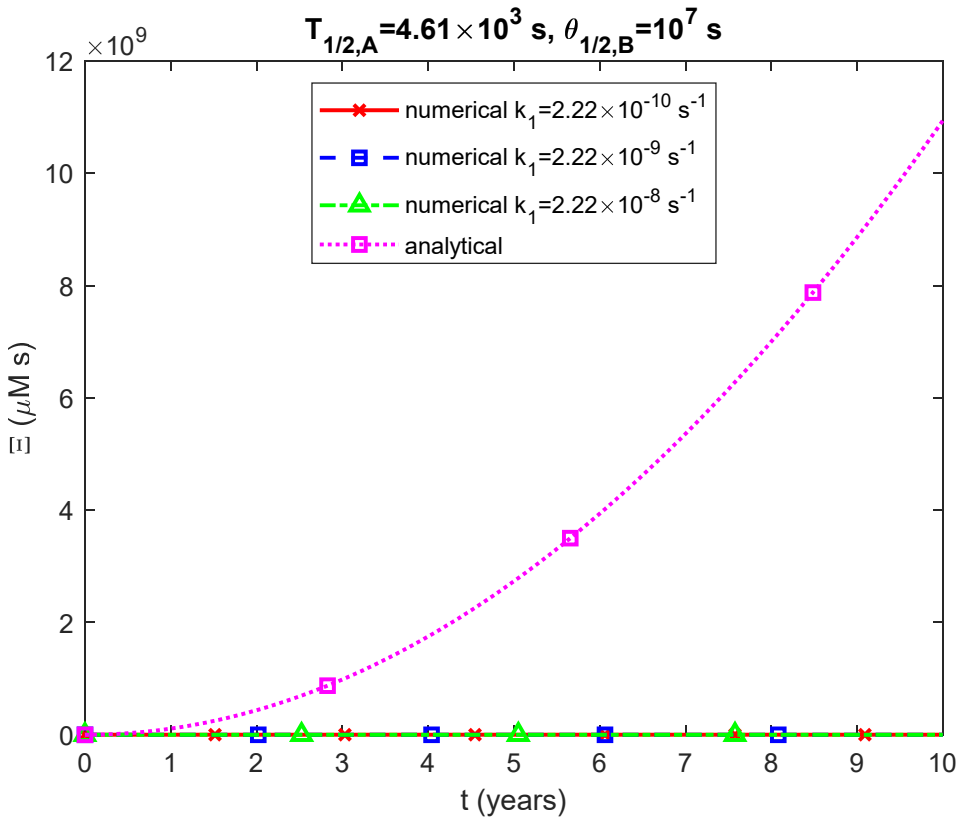
$T_{1/2,A}=4.61\times10^{3}$ s, $\theta_{1/2,B}=10^{7}$ s
$\times10^{9}$
numerical $k_1=2.22\times10^{-10}$ s^{-1}
numerical $k_1=2.22\times10^{-9}$ s^{-1}
numerical $k_1=2.22\times10^{-8}$ s^{-1}
analytical
Ξ (μM s)
t (years)

(b)

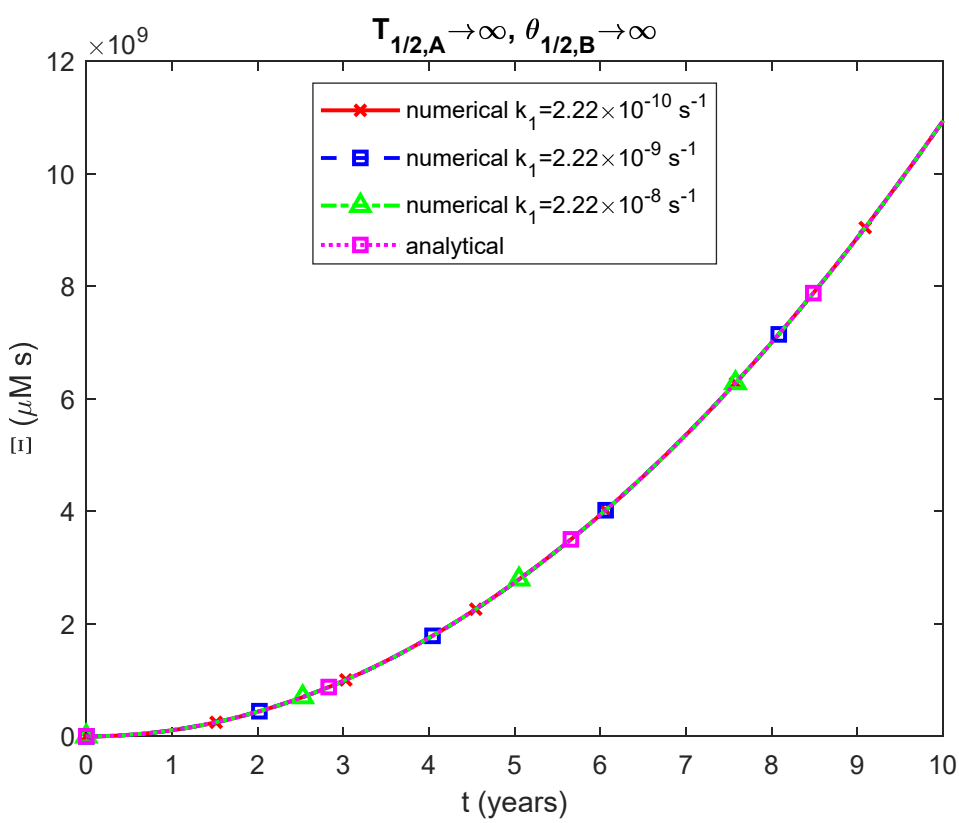
$T_{1/2,A}\rightarrow\infty$, $\theta_{1/2,B}\rightarrow\infty$
$\times10^{9}$
numerical $k_1=2.22\times10^{-10}$ s^{-1}
numerical $k_1=2.22\times10^{-9}$ s^{-1}
numerical $k_1=2.22\times10^{-8}$ s^{-1}
analytical
Ξ (μM s)
t (years)

Figure 2

(a)

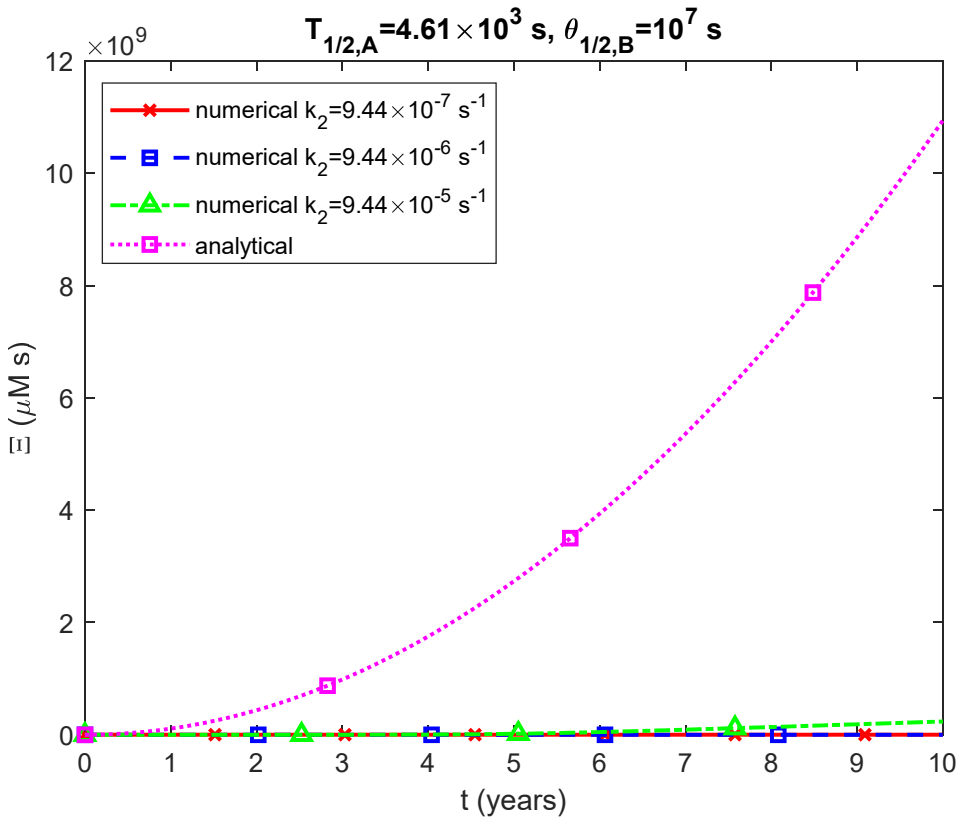
$T_{1/2,A}=4.61\times10^3$ s, $\theta_{1/2,B}=10^7$ s
$\times10^9$
numerical $k_2=9.44\times10^{-7}$ s^{-1}
numerical $k_2=9.44\times10^{-6}$ s^{-1}
numerical $k_2=9.44\times10^{-5}$ s^{-1}
analytical
Ξ (μM s)
t (years)

(b)

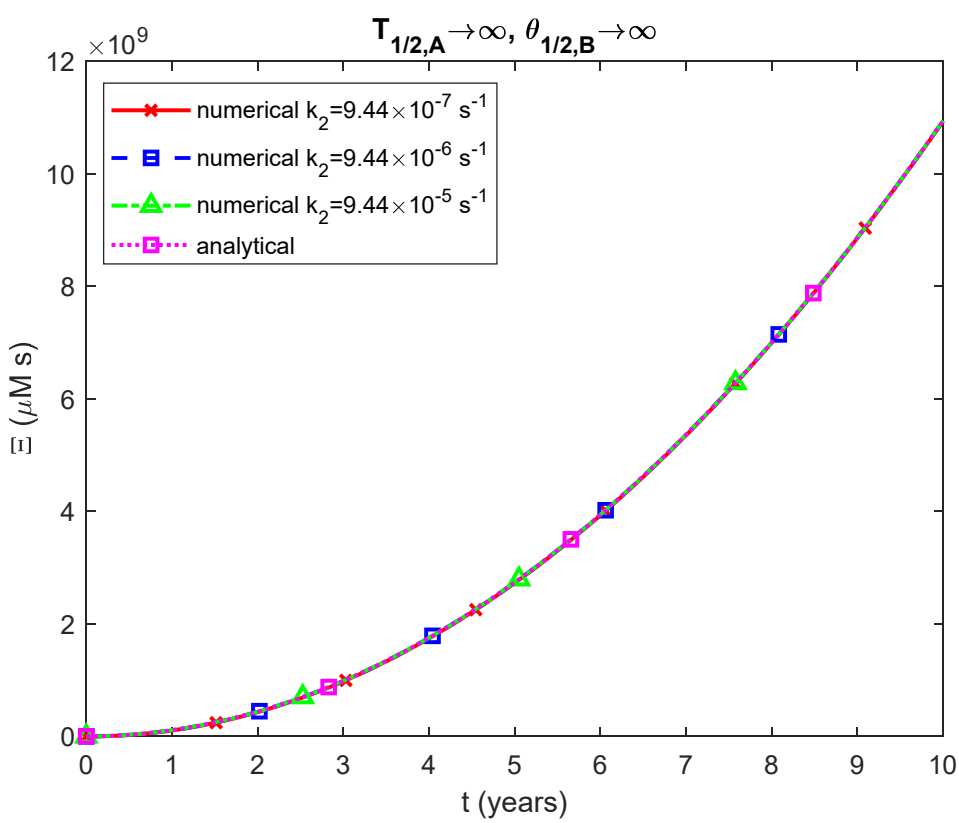
$T_{1/2,A}\to\infty$, $\theta_{1/2,B}\to\infty$
$\times10^9$
numerical $k_2=9.44\times10^{-7}$ s^{-1}
numerical $k_2=9.44\times10^{-6}$ s^{-1}
numerical $k_2=9.44\times10^{-5}$ s^{-1}
analytical
Ξ (μM s)
t (years)

Figure 3

(a)

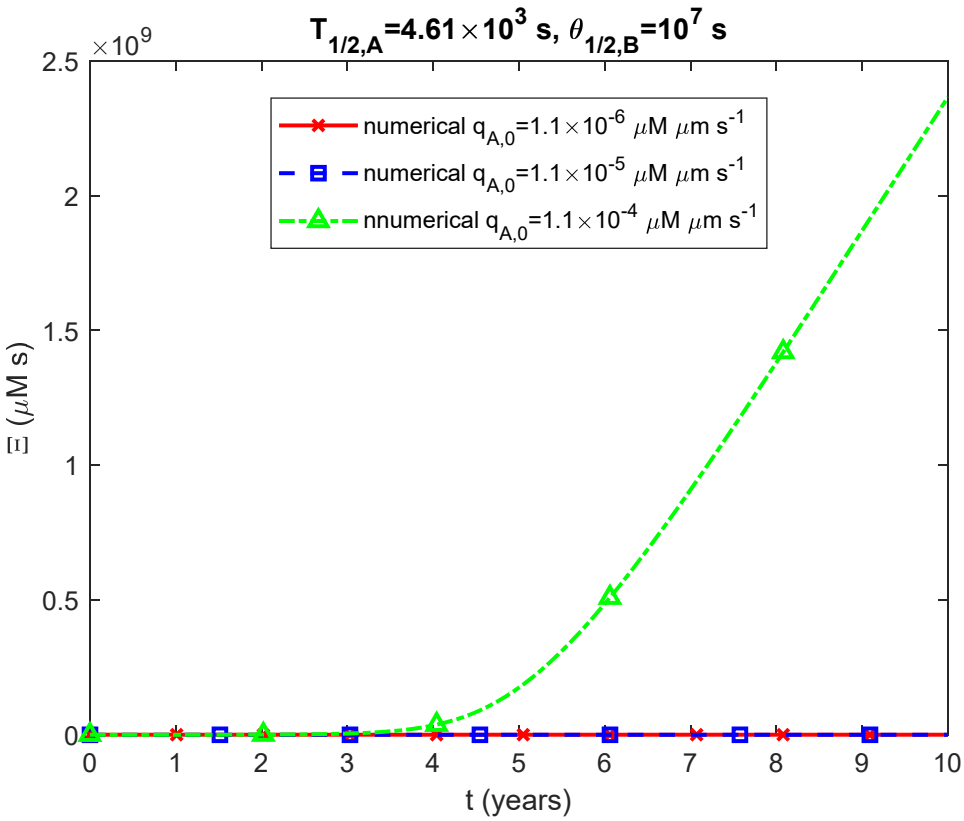
T1/2,A=4.61×10^3 s, θ1/2,B=10^7 s
×10^9
numerical qA,0=1.1×10^-6 μM μm s^-1
numerical qA,0=1.1×10^-5 μM μm s^-1
nnumerical qA,0=1.1×10^-4 μM μm s^-1
Ξ (μM s)
t (years)

(b)

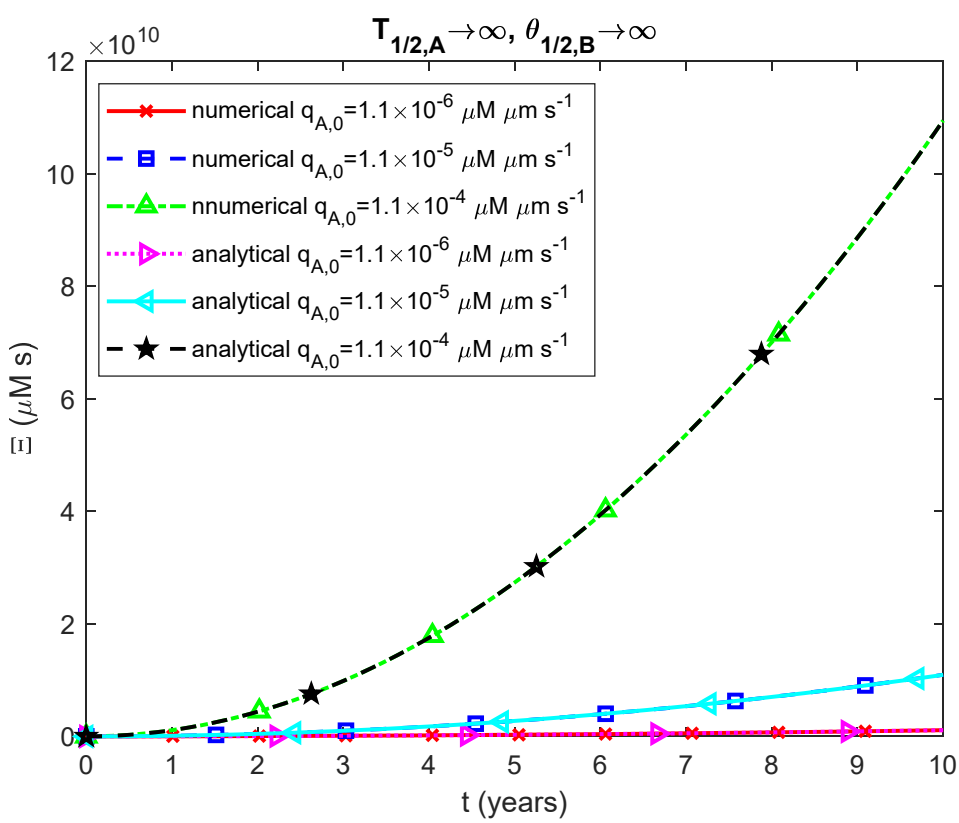
T1/2,A→∞, θ1/2,B→∞
×10^10
numerical qA,0=1.1×10^-6 μM μm s^-1
numerical qA,0=1.1×10^-5 μM μm s^-1
nnumerical qA,0=1.1×10^-4 μM μm s^-1
analytical qA,0=1.1×10^-6 μM μm s^-1
analytical qA,0=1.1×10^-5 μM μm s^-1
analytical qA,0=1.1×10^-4 μM μm s^-1
Ξ (μM s)
t (years)

Figure 4

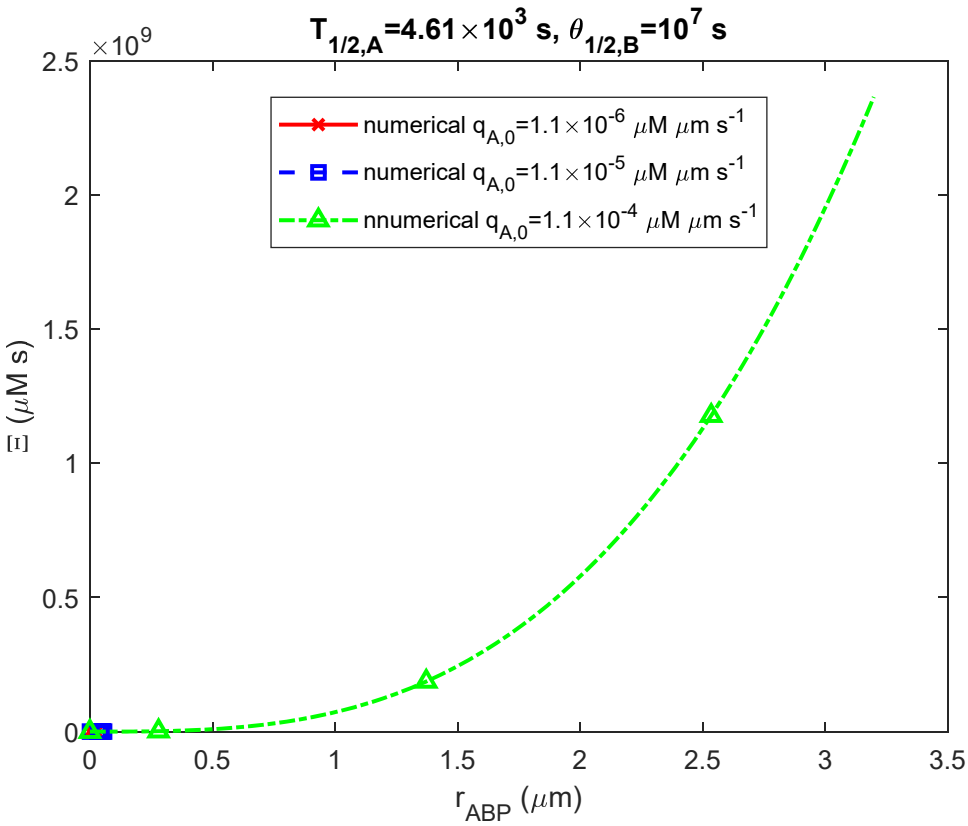
T1/2,A=4.61×10^3 s, θ1/2,B=10^7 s
×10^9
2.5
2
1.5
1
0.5
0
[I] (μM s)
numerical qA,0=1.1×10^-6 μM μm s^-1
numerical qA,0=1.1×10^-5 μM μm s^-1
nnumerical qA,0=1.1×10^-4 μM μm s^-1
0
0.5
1
1.5
2
2.5
3
3.5
rABP (μm)

Figure 5

(a)

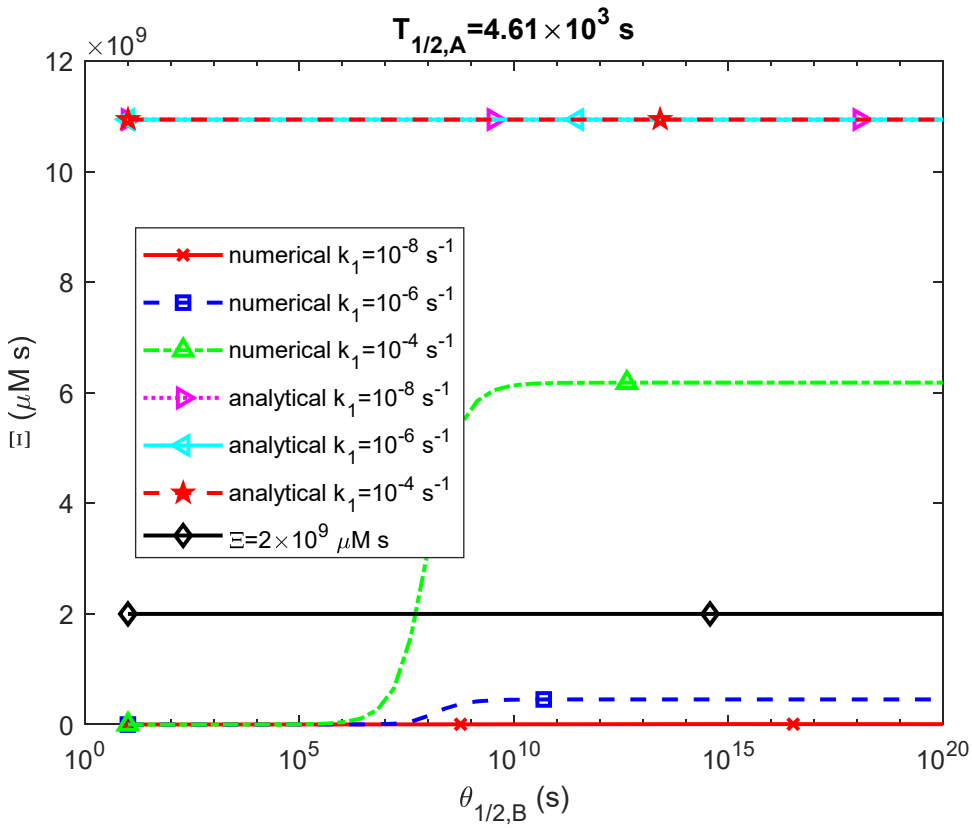
$T_{1/2,A}=4.61\times10^3$ s
$\times10^9$
12
10
8
6
4
2
0
Ξ (μM s)
numerical $k_1=10^{-8}$ s^{-1}
numerical $k_1=10^{-6}$ s^{-1}
numerical $k_1=10^{-4}$ s^{-1}
analytical $k_1=10^{-8}$ s^{-1}
analytical $k_1=10^{-6}$ s^{-1}
analytical $k_1=10^{-4}$ s^{-1}
$\Xi=2\times10^9$ μM s
10^0
10^5
10^{10}
10^{15}
10^{20}
$\theta_{1/2,B}$ (s)

(b)

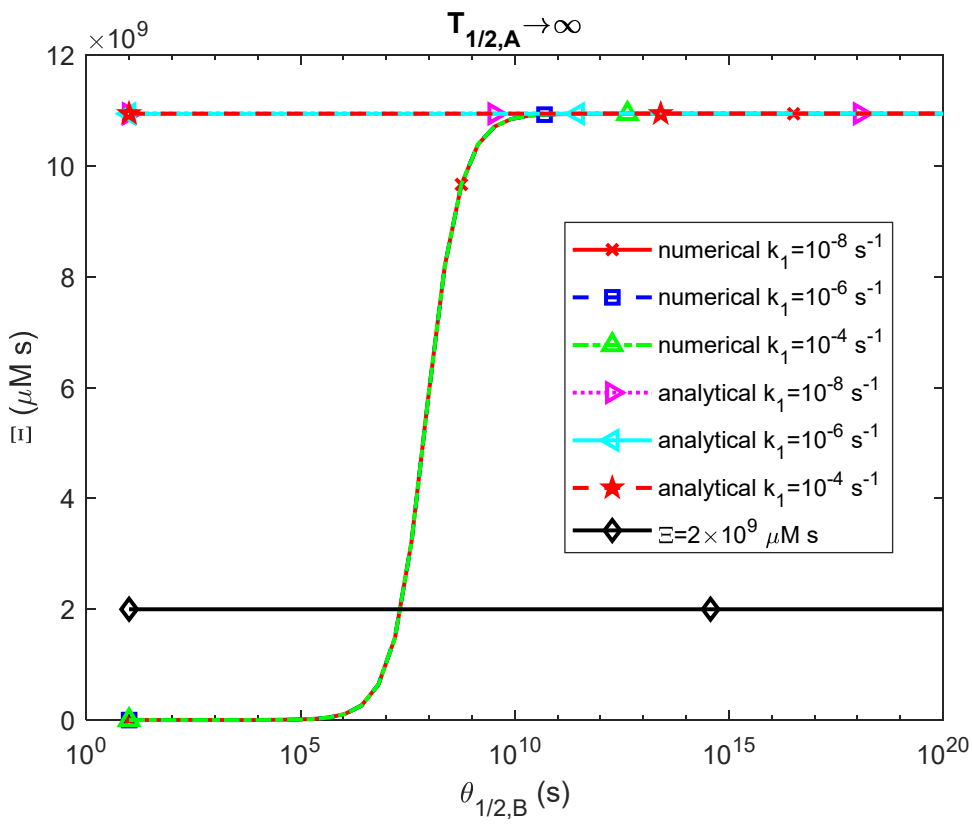
$T_{1/2,A}\rightarrow\infty$
$\times10^9$
12
10
8
6
4
2
0
Ξ (μM s)
numerical $k_1=10^{-8}$ s^{-1}
numerical $k_1=10^{-6}$ s^{-1}
numerical $k_1=10^{-4}$ s^{-1}
analytical $k_1=10^{-8}$ s^{-1}
analytical $k_1=10^{-6}$ s^{-1}
analytical $k_1=10^{-4}$ s^{-1}
$\Xi=2\times10^9$ μM s
10^0
10^5
10^{10}
10^{15}
10^{20}
$\theta_{1/2,B}$ (s)

Figure 6

(a)

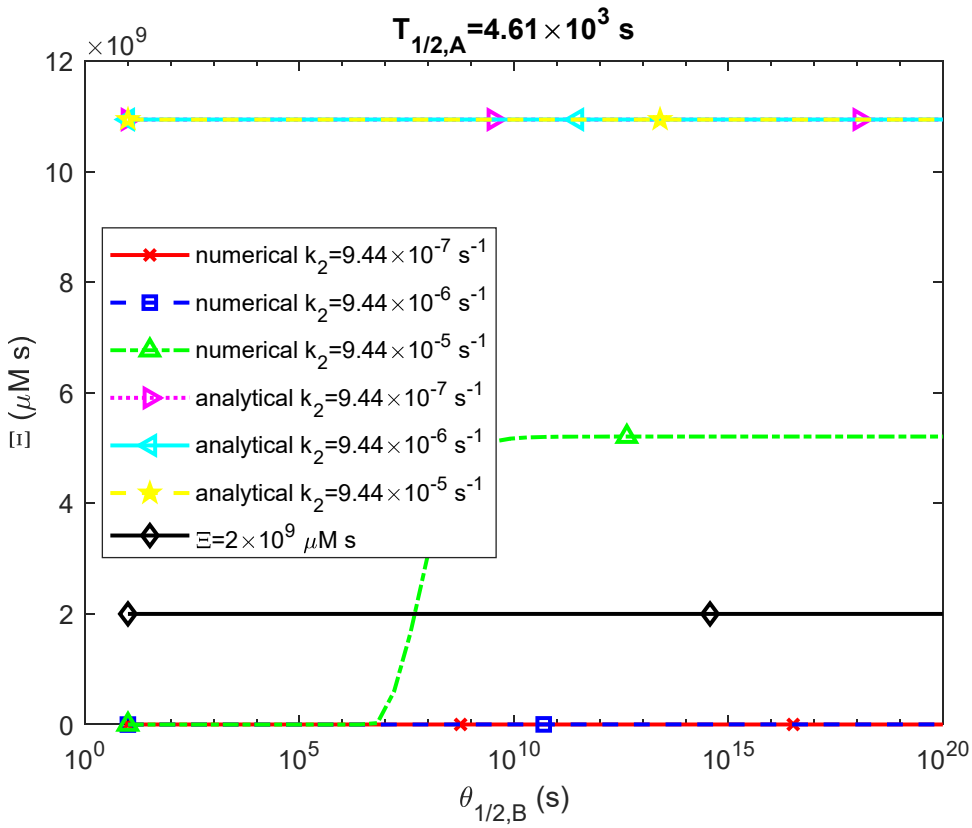
$T_{1/2,A}=4.61\times10^3$ s
$\times10^9$
12
10
8
6
4
2
0
Ξ (μM s)
numerical $k_2=9.44\times10^{-7}$ s^{-1}
numerical $k_2=9.44\times10^{-6}$ s^{-1}
numerical $k_2=9.44\times10^{-5}$ s^{-1}
analytical $k_2=9.44\times10^{-7}$ s^{-1}
analytical $k_2=9.44\times10^{-6}$ s^{-1}
analytical $k_2=9.44\times10^{-5}$ s^{-1}
$\Xi=2\times10^9$ μM s
10^0
10^5
10^{10}
10^{15}
10^{20}
$\theta_{1/2,B}$ (s)

(b)

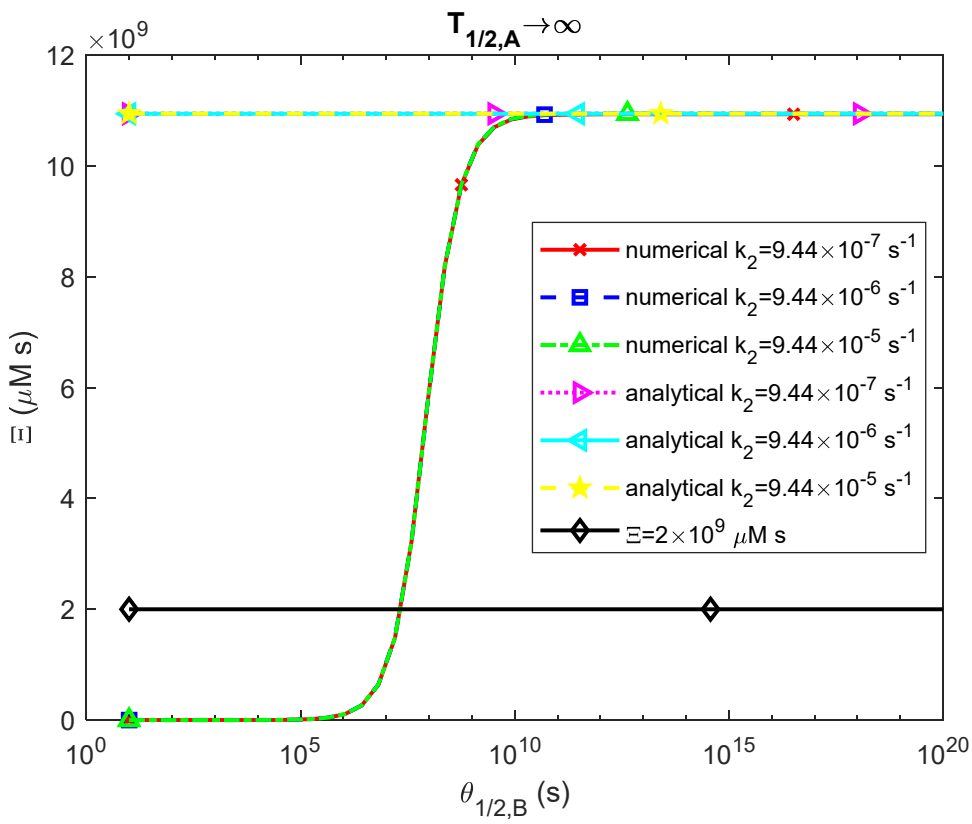
$T_{1/2,A}\rightarrow\infty$
$\times10^9$
12
10
8
6
4
2
0
Ξ (μM s)
numerical $k_2=9.44\times10^{-7}$ s^{-1}
numerical $k_2=9.44\times10^{-6}$ s^{-1}
numerical $k_2=9.44\times10^{-5}$ s^{-1}
analytical $k_2=9.44\times10^{-7}$ s^{-1}
analytical $k_2=9.44\times10^{-6}$ s^{-1}
analytical $k_2=9.44\times10^{-5}$ s^{-1}
$\Xi=2\times10^9$ μM s
10^0
10^5
10^{10}
10^{15}
10^{20}
$\theta_{1/2,B}$ (s)

Figure 7

(a)

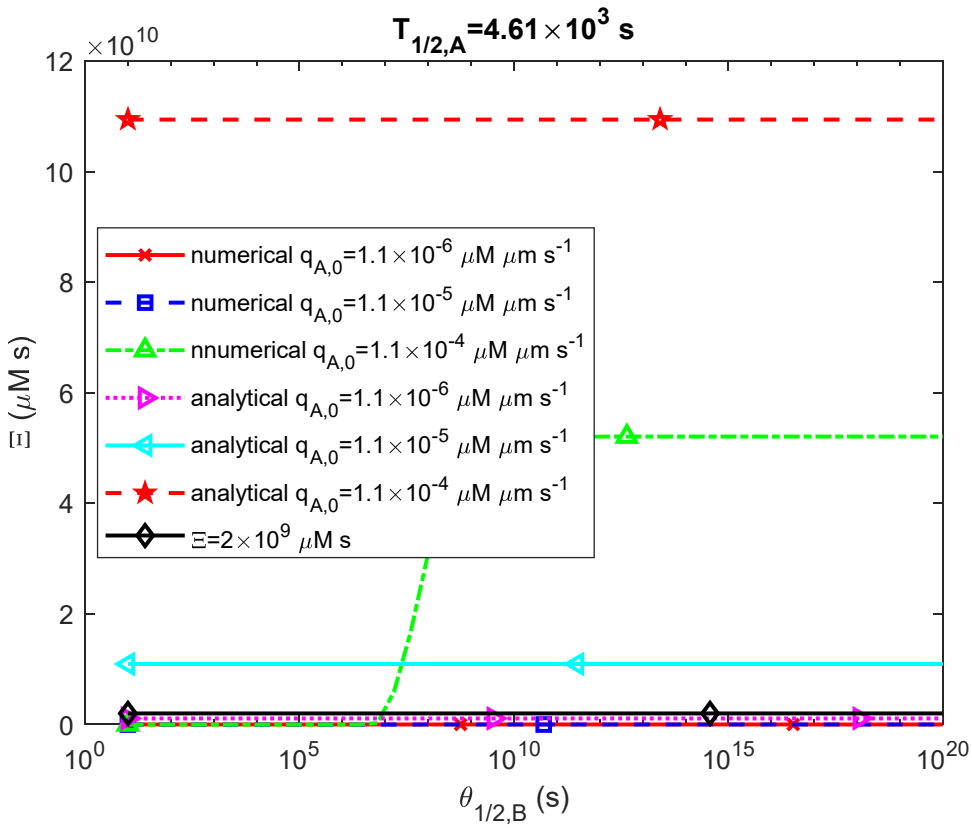
$T_{1/2,A}=4.61\times10^{3}$ s
$\times10^{10}$
numerical $q_{A,0}=1.1\times10^{-6}$ μM μm s^{-1}
numerical $q_{A,0}=1.1\times10^{-5}$ μM μm s^{-1}
nnumerical $q_{A,0}=1.1\times10^{-4}$ μM μm s^{-1}
analytical $q_{A,0}=1.1\times10^{-6}$ μM μm s^{-1}
analytical $q_{A,0}=1.1\times10^{-5}$ μM μm s^{-1}
analytical $q_{A,0}=1.1\times10^{-4}$ μM μm s^{-1}
$\Xi=2\times10^{9}$ μM s
Ξ (μM s)
$\theta_{1/2,B}$ (s)

(b)

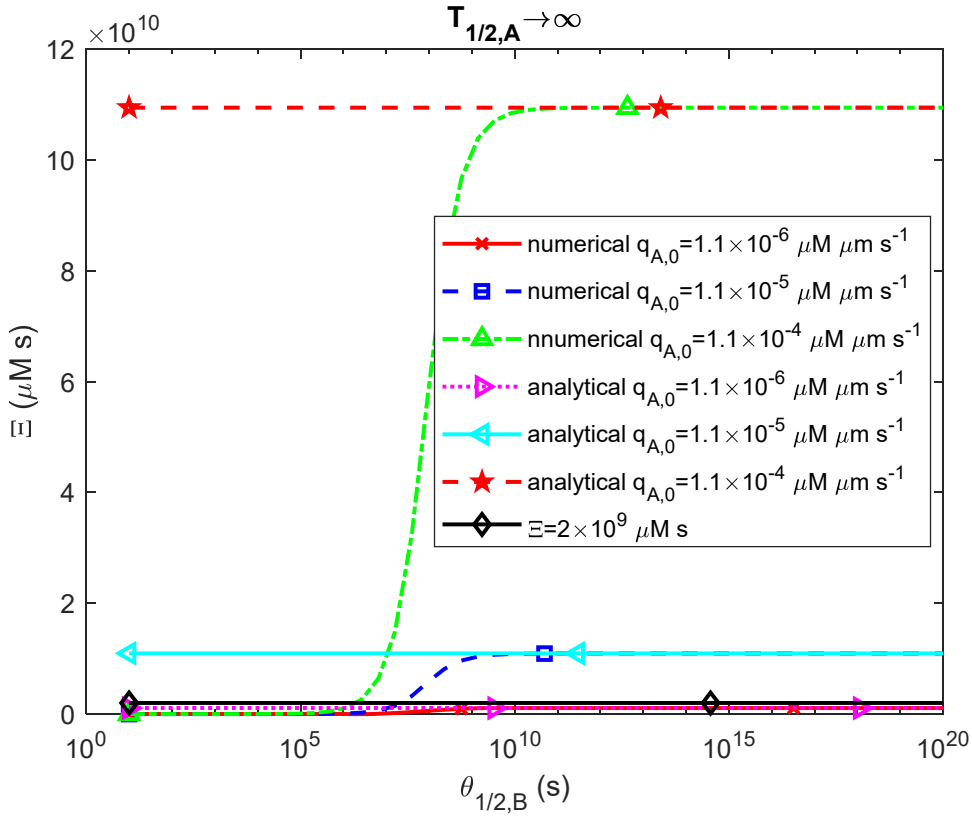
$T_{1/2,A}\rightarrow\infty$
$\times10^{10}$
numerical $q_{A,0}=1.1\times10^{-6}$ μM μm s^{-1}
numerical $q_{A,0}=1.1\times10^{-5}$ μM μm s^{-1}
nnumerical $q_{A,0}=1.1\times10^{-4}$ μM μm s^{-1}
analytical $q_{A,0}=1.1\times10^{-6}$ μM μm s^{-1}
analytical $q_{A,0}=1.1\times10^{-5}$ μM μm s^{-1}
analytical $q_{A,0}=1.1\times10^{-4}$ μM μm s^{-1}
$\Xi=2\times10^{9}$ μM s
Ξ (μM s)
$\theta_{1/2,B}$ (s)

Figure 8

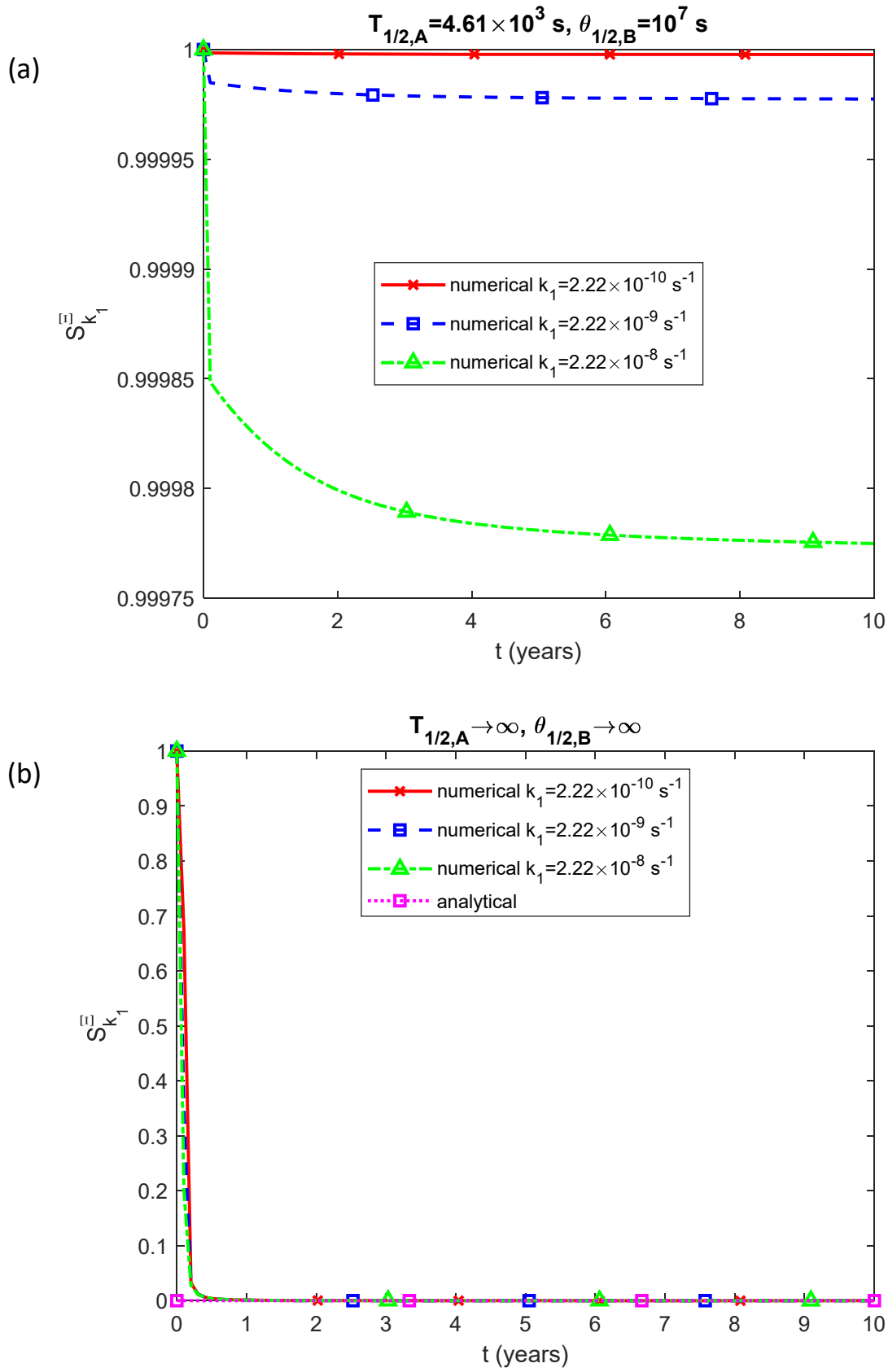
(a)
$T_{1/2,A}=4.61\times10^{3}$ s, $\theta_{1/2,B}=10^{7}$ s
numerical $k_1=2.22\times10^{-10}$ s^{-1}
numerical $k_1=2.22\times10^{-9}$ s^{-1}
numerical $k_1=2.22\times10^{-8}$ s^{-1}
$S^{[I]}_{k_1}$
t (years)
(b)
$T_{1/2,A}\rightarrow\infty$, $\theta_{1/2,B}\rightarrow\infty$
numerical $k_1=2.22\times10^{-10}$ s^{-1}
numerical $k_1=2.22\times10^{-9}$ s^{-1}
numerical $k_1=2.22\times10^{-8}$ s^{-1}
analytical
$S^{[I]}_{k_1}$
t (years)

Figure 9

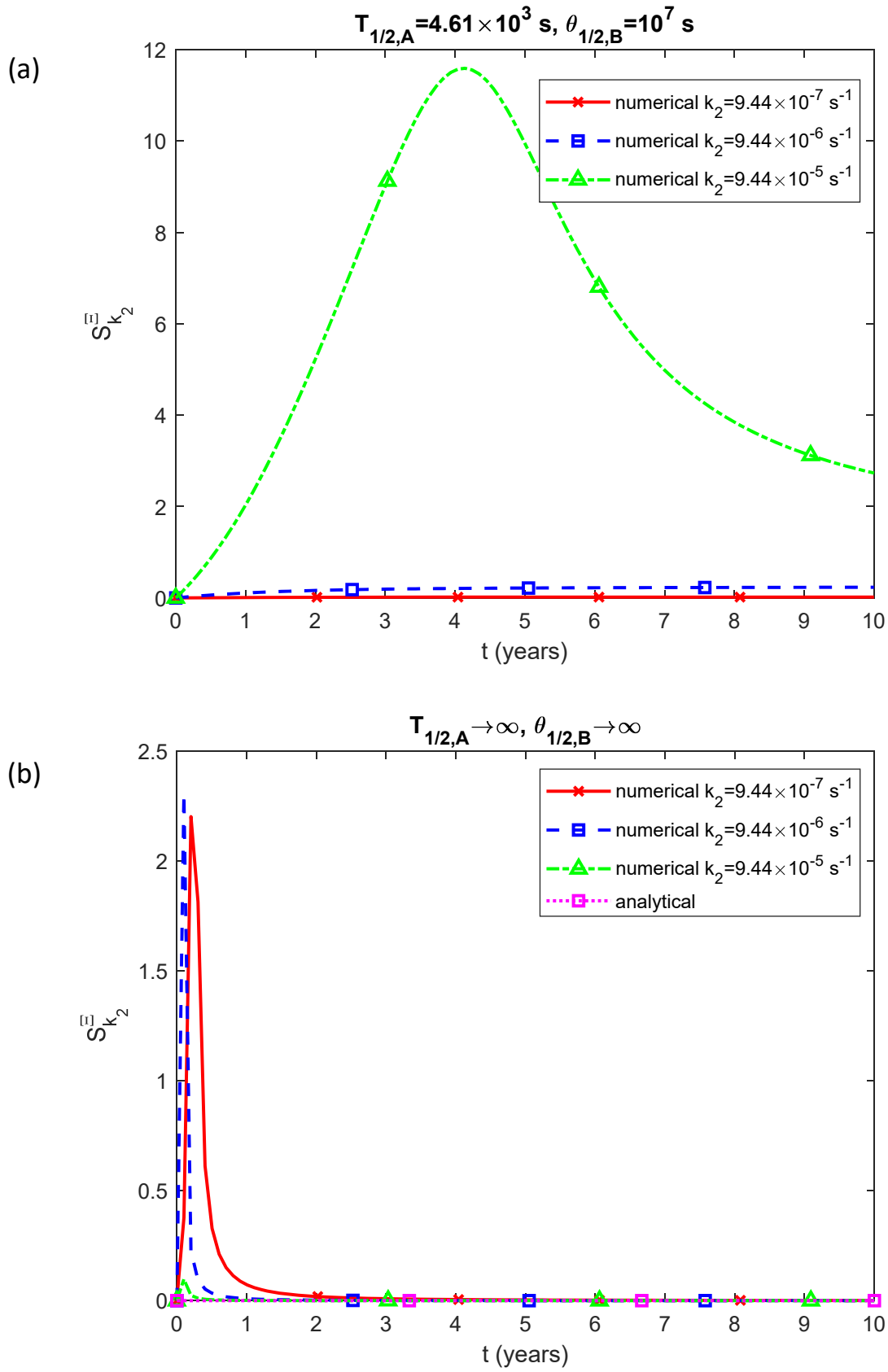
(a)
$T_{1/2,A}=4.61\times10^{3}$ s, $\theta_{1/2,B}=10^{7}$ s
numerical $k_2=9.44\times10^{-7}$ s^{-1}
numerical $k_2=9.44\times10^{-6}$ s^{-1}
numerical $k_2=9.44\times10^{-5}$ s^{-1}
$S^{[I]}_{k_2}$
t (years)
(b)
$T_{1/2,A}\rightarrow\infty$, $\theta_{1/2,B}\rightarrow\infty$
numerical $k_2=9.44\times10^{-7}$ s^{-1}
numerical $k_2=9.44\times10^{-6}$ s^{-1}
numerical $k_2=9.44\times10^{-5}$ s^{-1}
analytical
$S^{[I]}_{k_2}$
t (years)

Figure 10

(a)

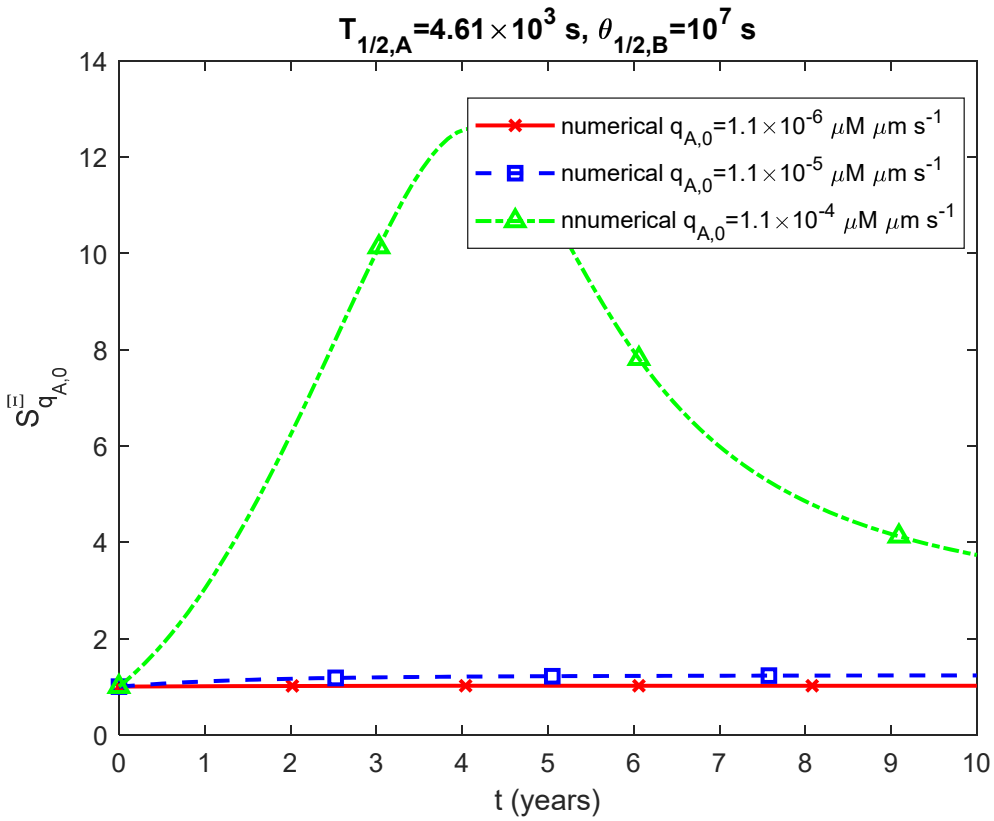
$T_{1/2,A}=4.61\times10^{3}$ s, $\theta_{1/2,B}=10^{7}$ s
numerical $q_{A,0}=1.1\times10^{-6}$ μM μm s^{-1}
numerical $q_{A,0}=1.1\times10^{-5}$ μM μm s^{-1}
nnumerical $q_{A,0}=1.1\times10^{-4}$ μM μm s^{-1}
$S^{[I]}_{q_{A,0}}$
t (years)

(b)

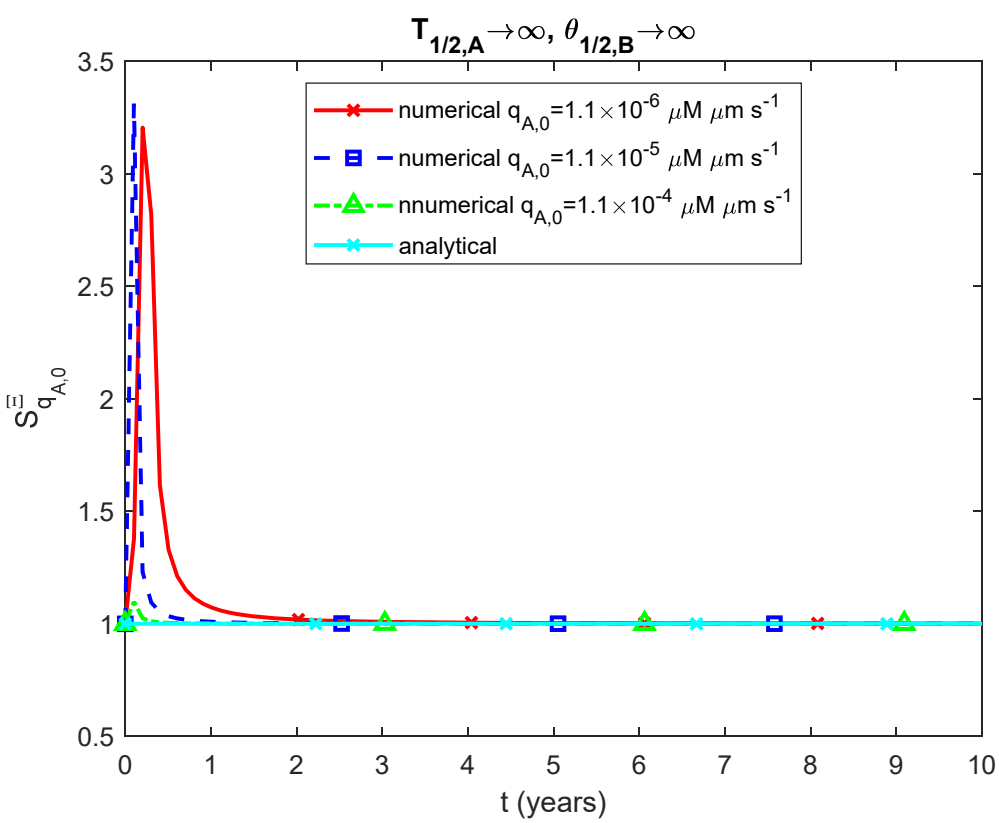
$T_{1/2,A}\rightarrow\infty$, $\theta_{1/2,B}\rightarrow\infty$
numerical $q_{A,0}=1.1\times10^{-6}$ μM μm s^{-1}
numerical $q_{A,0}=1.1\times10^{-5}$ μM μm s^{-1}
nnumerical $q_{A,0}=1.1\times10^{-4}$ μM μm s^{-1}
analytical
$S^{[I]}_{q_{A,0}}$
t (years)

Figure 11

A criterion characterizing accumulated neurotoxicity of Aβ oligomers in Alzheimer's disease

Andrey V Kuznetsov

Department of Mechanical and Aerospace Engineering, North Carolina State University,

Raleigh, NC 27695-7910, USA; e-mail: avkuznet@ncsu.edu

Supplemental Materials

S1. Dimensionless equations

S1.1. Dimensionless form of Eqs. (4)-(8)

The model described by Eqs. (4)-(7) is reformulated in dimensionless form as shown below, where asterisks denote dimensionless quantities:

$$\frac{\partial C_A^*}{\partial t^*} = -C_A^* - C_A^* C_B^* - C_A^* \frac{\ln(2)}{T_{1/2,A}^*} + q_{A,0}^* \tag{S1}$$

$$\frac{\partial C_B^*}{\partial t^*} = C_A^* + C_A^* C_B^* - C_B^* \frac{\ln(2)}{T_{1/2,B}^*} - C_B^* \frac{\ln(2)}{\theta_{1/2,B}^*} \tag{S2}$$

$$\frac{\partial C_D^*}{\partial t^*} = C_B^* \frac{\ln(2)}{\theta_{1/2,B}^*} - C_D^* \frac{\ln(2)}{T_{1/2,D}^*} \tag{S3}$$

At $t^* = 0$: $C_A^* = 0$, $C_B^* = 0$, $C_D^* = 0$ (S4)

The independent dimensionless variable in the model is given in Table S1, with the dependent dimensionless variables summarized in Table S2. Table S3 provides a summary of the dimensionless parameters used in the model.

The parameter representing the accumulated toxicity of Aβ, as given by Eq. (8), can be reformulated in terms of dimensions quantities as follows:

$$\Xi^*\left(t^*\right) = \int_0^{t^*} C_B^*\left(\hat{t}^*\right) d\hat{t}^* \tag{S5}$$

where

$$\Xi^* = \Xi k_2 \tag{S6}$$

S1.2. Analytical solution of Eqs. (15) and (16)

Combining Eqs. (15) and (16) yields

$$\frac{dC_A}{dt}+\frac{dC_B}{dt}=\frac{q_{A,0}}{L} \tag{S7}$$

By integrating Eq. (S7) over time and applying the initial conditions specified in Eq. (7a,b), the following result is derived:

$$C_A+C_B=\frac{q_{A,0}}{L}t \tag{S8}$$

The increase in C_A+C_B over time is due to the influx of Aβ monomers through the left boundary of the CV. By substituting Eq. (S8) into Eq. (16) to eliminate C_A, the following expression is obtained:

$$\frac{dC_B}{dt}=k_1\left(\frac{q_{A,0}}{L}t-C_B\right)+k_2\left(\frac{q_{A,0}}{L}t-C_B\right)C_B \tag{S9}$$

Eq. (S9) is similar to the equation studied in [31]. To obtain the exact solution of Eq. (S9) with the initial condition specified in Eq. (7b), Mathematica 13.3 (Wolfram Research, Champaign, IL) was utilized, employing the DSolve function followed by the FullSimplify function. The derived solution is as follows:

$$C_B=\frac{k_1}{k_2}\times\left(-1+\frac{\left(k_2q_{A,0}\right)^{1/2}\exp\left[k_1t+\frac{k_2q_{A,0}}{2L}t^2\right]}{\left(k_2q_{A,0}\right)^{1/2}-\left(2L\right)^{1/2}k_1\left(F\left(\frac{k_1L^{1/2}}{\left(2k_2q_{A,0}\right)^{1/2}}\right)\right)-\exp\left[k_1t+\frac{k_2q_{A,0}}{2L}t^2\right]F\left[\frac{k_1L+k_2q_{A,0}t}{\left(2k_2q_{A,0}L\right)^{1/2}}\right]}\right) \tag{S10}$$

In this equation, $F(x)$ represents Dawson's integral:

$$F(x)=\frac{1}{2}\sqrt{\pi}\,e^{-x^2}\,erfi(x) \tag{S11}$$

where $erfi(x)$ is the imaginary error function.

As $t \to 0$, Eq. (S10) shows that $C_B \to \frac{k_1 q_{A,0} t^2}{2L}$, suggesting that at early times, the concentration of Aβ aggregates is linearly dependent on the nucleation rate constant, k_1. Using Eq. (S8), the expression for C_A can be derived as:

$$C_A = \frac{q_{A,0}}{L} t - C_B \tag{S12}$$

To estimate the maximum possible plaque radius, one can assume that all aggregates deposit into plaques. However, this assumption conflicts with the condition $\theta_{1/2,B} \to \infty$, so the maximum radius would be reached at some finite value of $\theta_{1/2,B}$ (but not at zero).

If the approximate solution given by Eqs. (18) and (19) is used, the following result is obtained. Renaming C_B given in Eq. (19) and substituting it into Eq. (14) yield

$$r_{ABP} = \left(\frac{3}{2\pi} \frac{L^2}{a_{21}} \frac{MWq_{A,0}}{\rho} \right)^{1/3} t^{1/3} \tag{S13}$$

which represents the "cube root of time" hypothesis, originally formulated by [14].

S1.3. Numerical solution

Eqs. (4)–(6), along with their initial conditions in Eq. (7), were numerically solved using MATLAB's ODE45 solver (MATLAB R2020b, MathWorks, Natick, MA, USA), which is widely recognized for its accuracy and robustness. The relative and absolute tolerances, RelTol and AbsTol, were set to 1e-10 to ensure high precision in the solutions.

S2. Tables

Table S1. Dimensionless independent variables used in the model.

Symbol	Definition
t^*	$t k_1$

Table S2. Dimensionless dependent variables used in the model.

Symbol	Definition
C_A^*	$C_A k_2 / k_1$
C_B^*	$C_B k_2 / k_1$
C_D^*	$C_D k_2 / k_1$

Table S3. Dimensionless parameters used in the model.

Symbol	Definition
$q_{A,0}^*$	$q_{A,0} k_2 / \left(k_1^2 L\right)$
t_f^*	$t_f k_1$
$T_{1/2,A}^*$	$T_{1/2,A} k_1$
$T_{1/2,B}^*$	$T_{1/2,B} k_1$
$T_{1/2,D}^*$	$T_{1/2,D} k_1$
$\theta_{1/2,B}^*$	$\theta_{1/2,B} k_1$
ρ^*	$\frac{\rho}{MW} a_{21} \frac{k_2}{k_1}$

S3. Supplementary figures

(a)

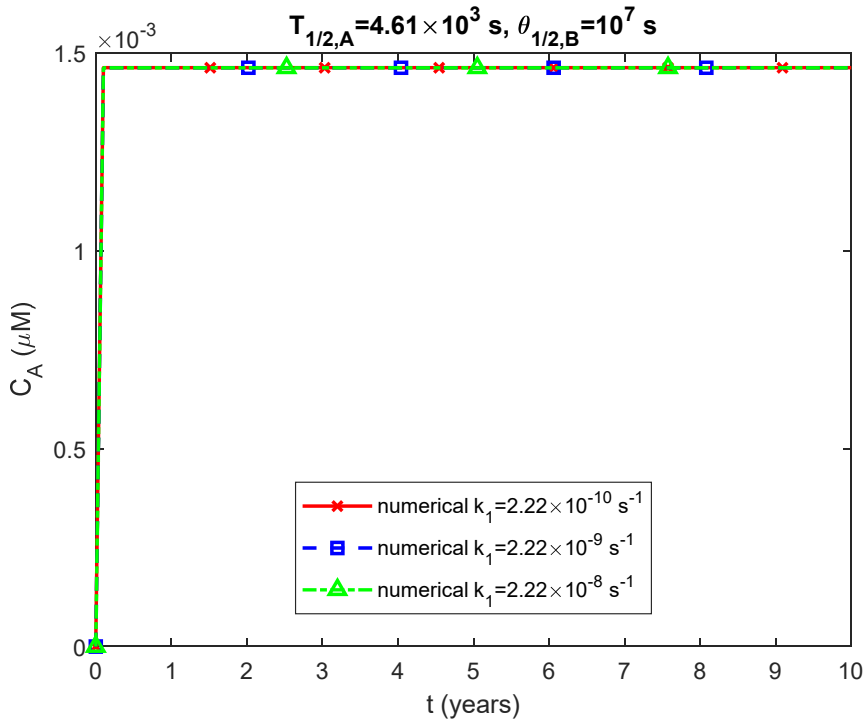
$T_{1/2,A}$=4.61×10^3 s, $\theta_{1/2,B}$=10^7 s
×10^-3
1.5
1
0.5
0
C_A (μM)
0 1 2 3 4 5 6 7 8 9 10
t (years)
numerical k_1=2.22×10^-10 s^-1
numerical k_1=2.22×10^-9 s^-1
numerical k_1=2.22×10^-8 s^-1

(b)

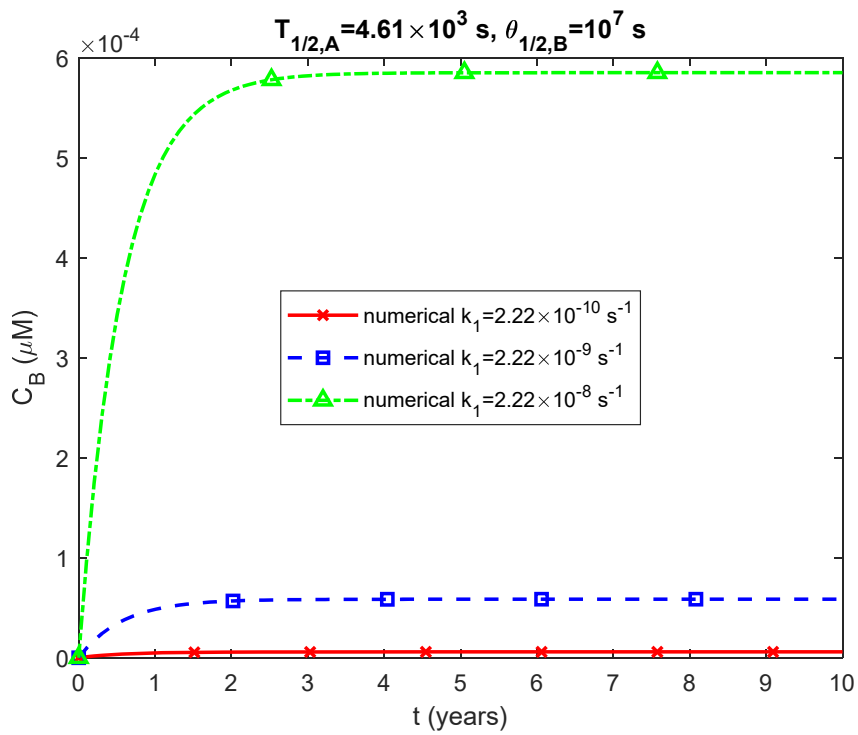
$T_{1/2,A}$=4.61×10^3 s, $\theta_{1/2,B}$=10^7 s
×10^-4
6
5
4
3
2
1
0
C_B (μM)
0 1 2 3 4 5 6 7 8 9 10
t (years)
numerical k_1=2.22×10^-10 s^-1
numerical k_1=2.22×10^-9 s^-1
numerical k_1=2.22×10^-8 s^-1

Fig. S1. Molar concentration of Aβ monomers, C_A (a); and free Aβ aggregates, C_B (b) as a function of time (in years). Results are shown for three different values of k_1. The scenario with a finite half-life of Aβ monomers ($T_{1/2,A} = 4.61 \times 10^3$ s) and an intermediate value of half-deposition time of Aβ aggregates into senile plaques ($\theta_{1/2,B} = 10^7$ s).

(a)

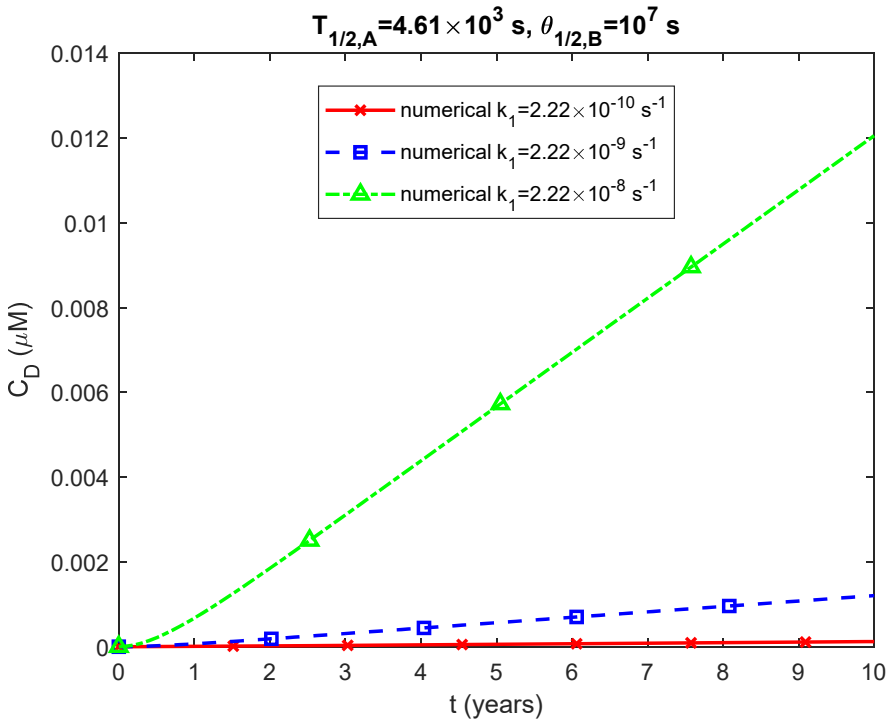

(b)

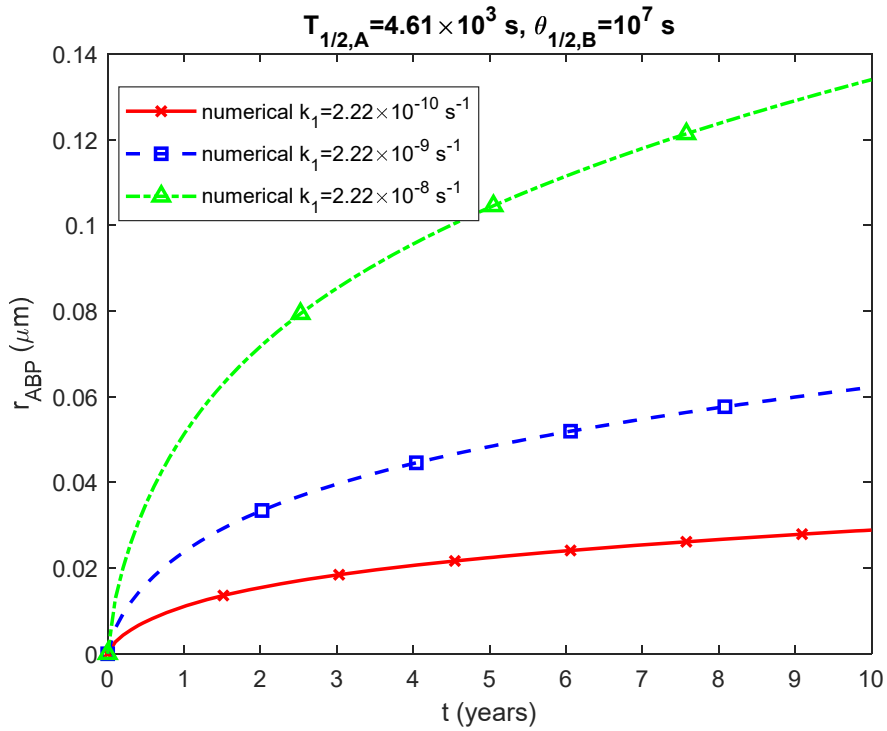

Fig. S2. Molar concentration of Aβ aggregates deposited in plaques, C_D (a); and the radius of a growing Aβ plaque, r_{ABP} (b); as a function of time (in years). Results are shown for three different values of k_1. The scenario with a finite half-life of Aβ monomers ($T_{1/2,A} = 4.61\times10^3$ s) and an intermediate value of half-deposition time of Aβ aggregates into senile plaques ($\theta_{1/2,B} = 10^7$ s).

(a)

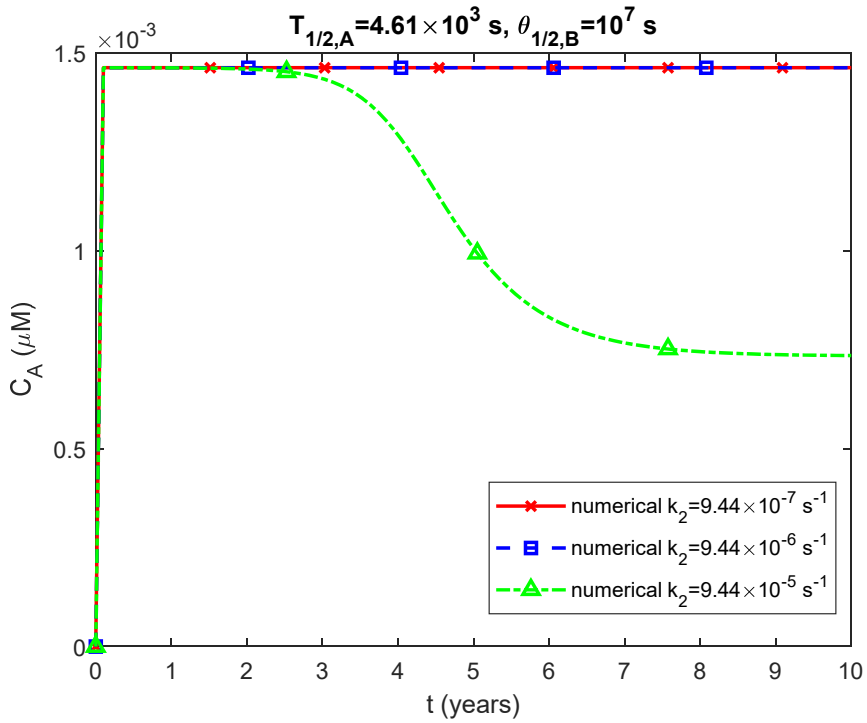
$T_{1/2,A}$=4.61×10^3 s, $\theta_{1/2,B}$=10^7 s
×10^-3
1.5
1
0.5
0
C_A (μM)
0 1 2 3 4 5 6 7 8 9 10
t (years)
numerical k_2=9.44×10^-7 s^-1
numerical k_2=9.44×10^-6 s^-1
numerical k_2=9.44×10^-5 s^-1

(b)

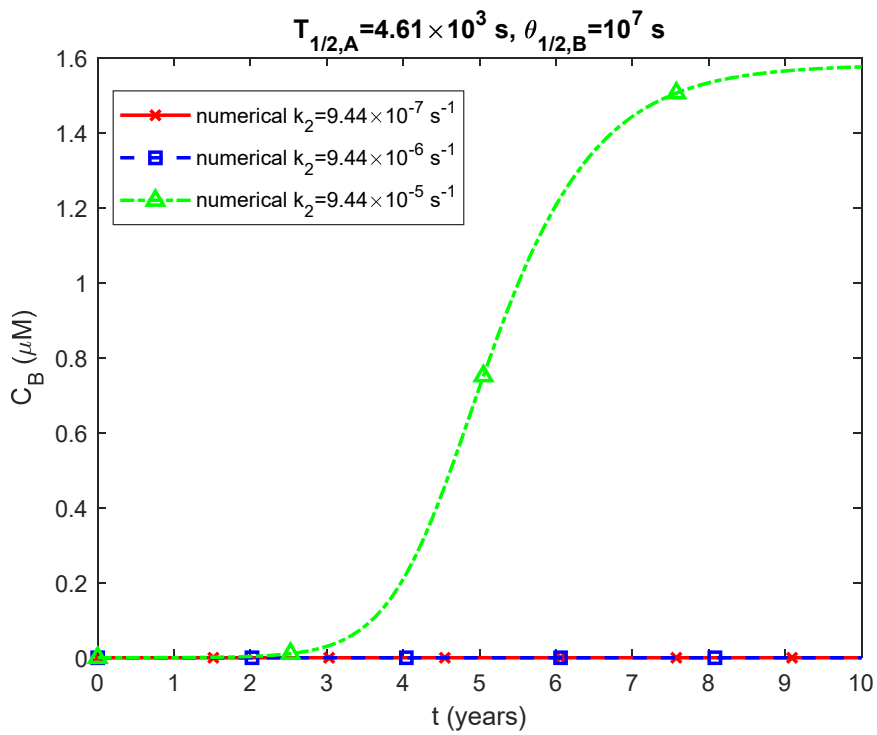
$T_{1/2,A}$=4.61×10^3 s, $\theta_{1/2,B}$=10^7 s
1.6
1.4
1.2
1
0.8
0.6
0.4
0.2
0
C_B (μM)
0 1 2 3 4 5 6 7 8 9 10
t (years)
numerical k_2=9.44×10^-7 s^-1
numerical k_2=9.44×10^-6 s^-1
numerical k_2=9.44×10^-5 s^-1

Fig. S3. Molar concentration of Aβ monomers, C_A (a); and free Aβ aggregates, C_B (b) as a function of time (in years). Results are shown for three different values of k_2. The scenario with a finite half-life of Aβ monomers ($T_{1/2,A} = 4.61 \times 10^3$ s) and an intermediate value of half-deposition time of Aβ aggregates into senile plaques ($\theta_{1/2,B} = 10^7$ s).

(a)

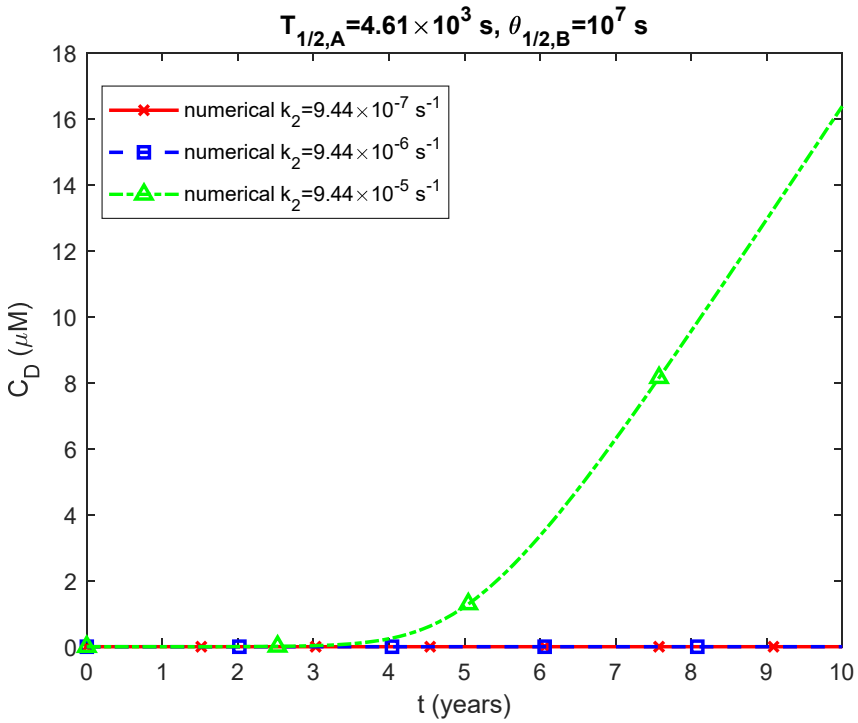

(b)

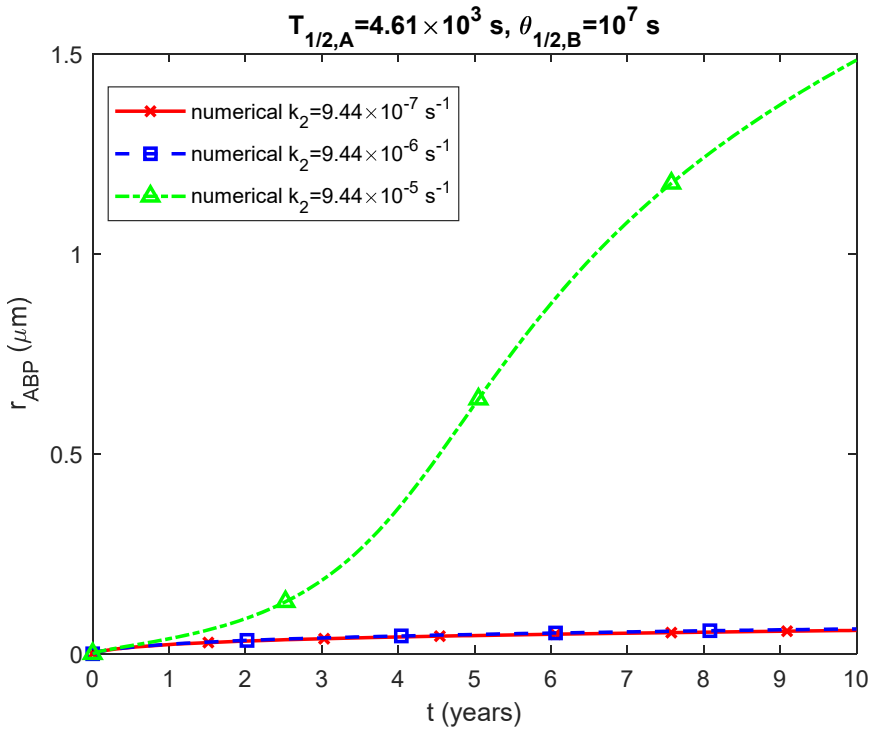

Fig. S4. Molar concentration of Aβ aggregates deposited in plaques, C_D (a); and the radius of a growing Aβ plaque, r_{ABP} (b); as a function of time (in years). Results are shown for three different values of k_2. The scenario with a finite half-life of Aβ monomers ($T_{1/2,A} = 4.61 \times 10^3$ s) and an intermediate value of half-deposition time of Aβ aggregates into senile plaques ($\theta_{1/2,B} = 10^7$ s).

(a)

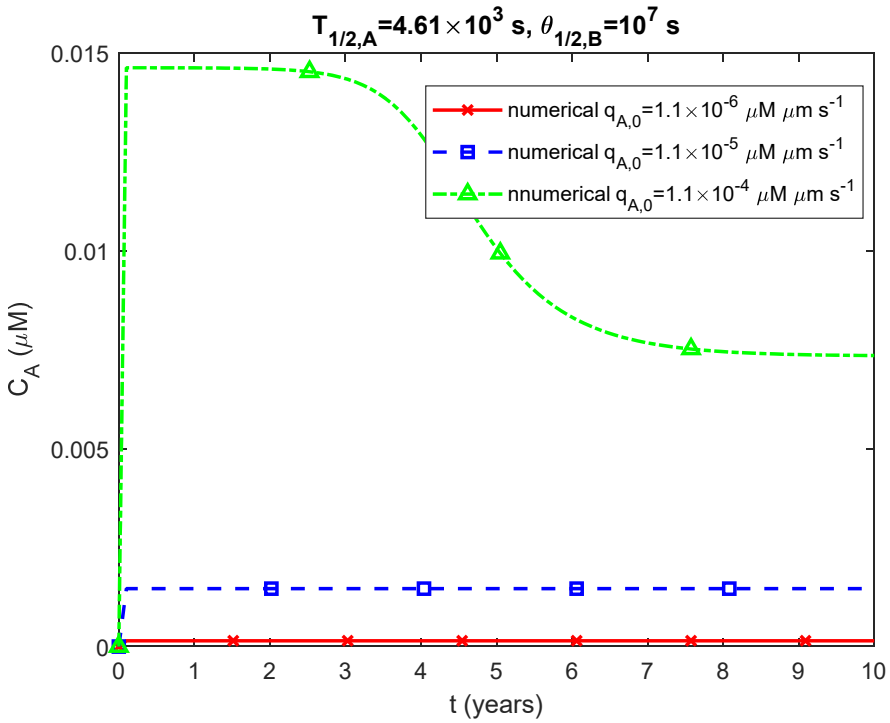
$T_{1/2,A}=4.61\times10^3$ s, $\theta_{1/2,B}=10^7$ s
numerical $q_{A,0}=1.1\times10^{-6}$ μM μm s^{-1}
numerical $q_{A,0}=1.1\times10^{-5}$ μM μm s^{-1}
nnumerical $q_{A,0}=1.1\times10^{-4}$ μM μm s^{-1}
C_A (μM)
t (years)

(b)

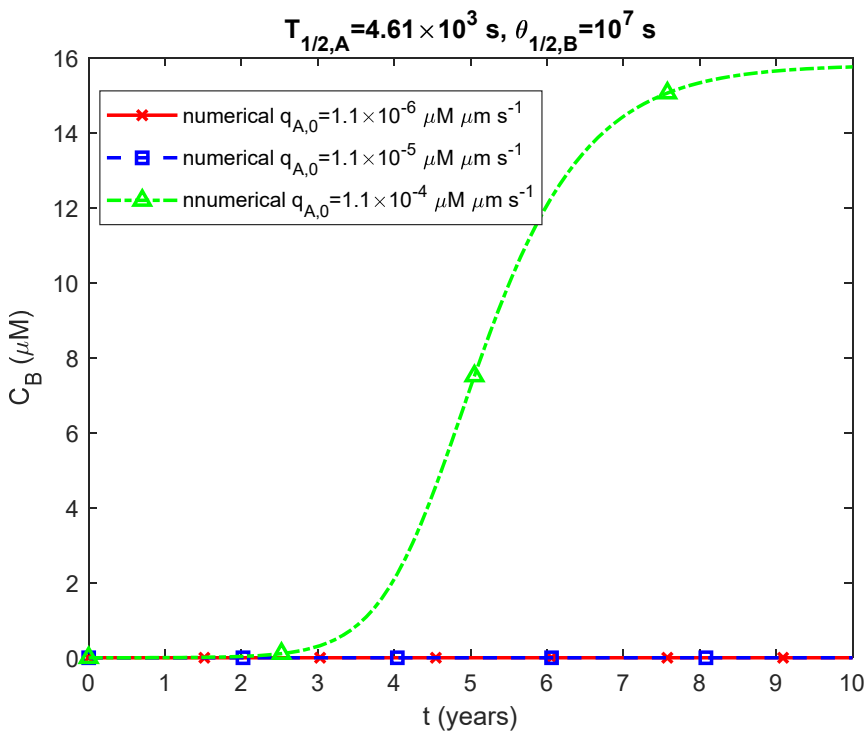
$T_{1/2,A}=4.61\times10^3$ s, $\theta_{1/2,B}=10^7$ s
numerical $q_{A,0}=1.1\times10^{-6}$ μM μm s^{-1}
numerical $q_{A,0}=1.1\times10^{-5}$ μM μm s^{-1}
nnumerical $q_{A,0}=1.1\times10^{-4}$ μM μm s^{-1}
C_B (μM)
t (years)

Fig. S5. Molar concentration of Aβ monomers, C_A (a); and free Aβ aggregates, C_B (b) as a function of time (in years). Results are shown for three different values of $q_{A,0}$. The scenario with a finite half-life of Aβ monomers ($T_{1/2,A} = 4.61 \times 10^3$ s) and an intermediate value of half-deposition time of Aβ aggregates into senile plaques ($\theta_{1/2,B} = 10^7$ s).

(a)

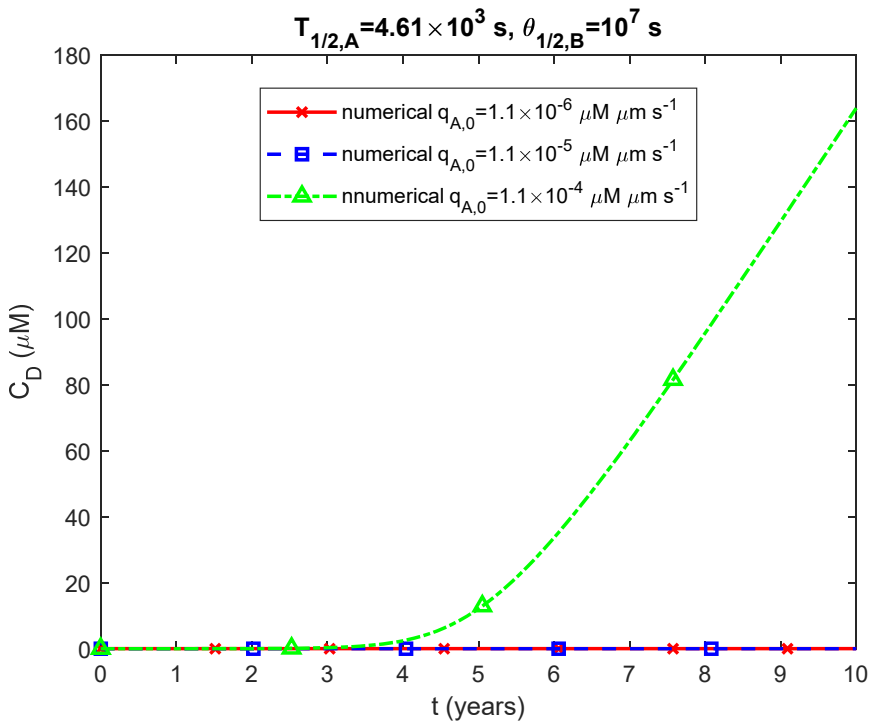

(b)

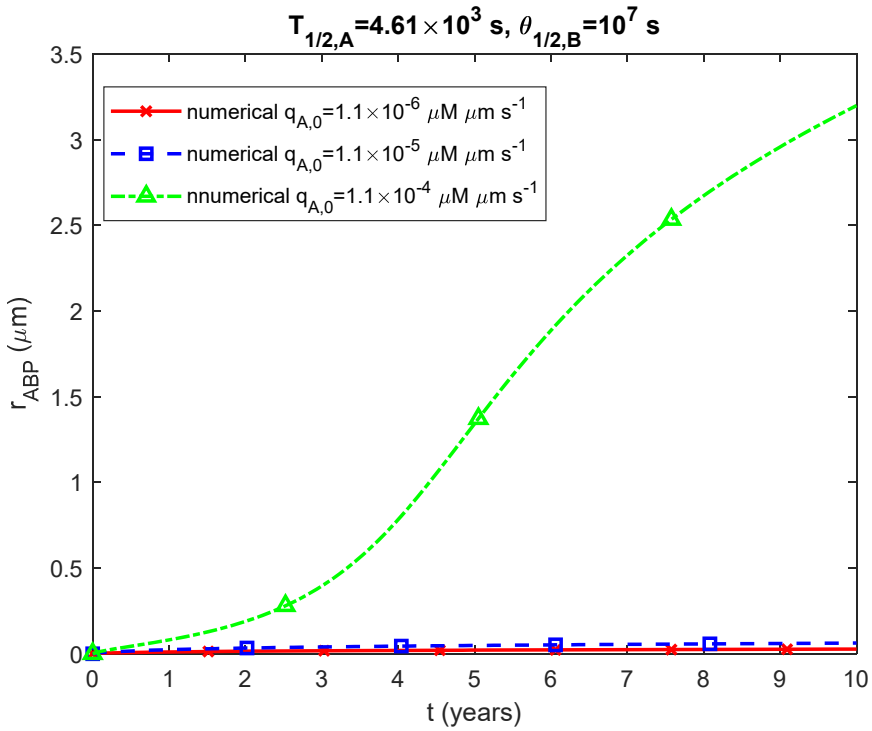

Fig. S6. Molar concentration of Aβ aggregates deposited in plaques, C_D (a); and the radius of a growing Aβ plaque, r_{ABP} (b); as a function of time (in years). Results are shown for three different values of $q_{A,0}$. The scenario with a finite half-life of Aβ monomers ($T_{1/2,A} = 4.61\times10^3$ s) and an intermediate value of half-deposition time of Aβ aggregates into senile plaques ($\theta_{1/2,B} = 10^7$ s).